Auditory Hair Cells and Spiral Ganglion Neurons Regenerate Synapses with Refined Release Properties In Vitro

Philippe F.Y. Vincent[1,2*], Eric D. Young[1,2,3,4], Albert S.B. Edge[5,6,7,8], Elisabeth Glowatzki[1,2,3*]

[1]The Center for Hearing and Balance, [2]Department of Otolaryngology Head and Neck Surgery, [3]Department of Neuroscience, [4]Department of Biomedical Engineering, The Johns Hopkins School of Medicine, Baltimore, Maryland, [5]Department of Otolaryngology, Harvard Medical School, [6]Eaton-Peabody Laboratory, Massachusetts Eye and Ear, Boston, Massachusetts, USA. [7]Program in Speech and Hearing Bioscience and Technology, Harvard Medical School, Boston, Massachusetts, USA. [8]Harvard Stem Cell Institute, Cambridge, Massachusetts, USA.

*Correspondence: Philippe Vincent, pvincen3@jhmi.edu and Elisabeth Glowatzki, eglowat1@jhmi.edu

AUTHOR CONTRIBUTIONS: PV, AE and EG designed research; PV performed research; PV, EY analyzed data; PV and EG wrote the manuscript; EY and AE edited the manuscript.

ACKNOWLEDGEMENTS: This work was supported by the National Institute on Deafness and Other Communication Disorders Grants R01DC006476 to EG, the David M. Rubenstein Fund for Hearing Research to EG, the Geraldine Dietz Fox Endowed Research Fund to EG, the Hearing Health Foundation grant to PV, R01 DC007174 to AE. We thank Dr. Mingji Tong, Eaton Peabody Laboratory, Massachusetts Eye and Ear, Boston MA, for training in cell culture models with regenerated synapses.

CONFLICT OF INTEREST: Authors report no conflict of interest.

ORCID: 0000-0001-7712-7198 (for PV) and 0000-0003-3135-658X (for EG)

ABSTRACT

Ribbon synapses between inner hair cells (IHCs) and type I spiral ganglion neurons (SGNs) in the inner ear are damaged by noise trauma and with aging, causing 'synaptopathy 'and hearing loss. Co-cultures of neonatal denervated organs of Corti and newly introduced SGNs have been developed to find strategies for improving IHC synapse regeneration, but evidence of the physiological normality of regenerated synapses is missing. This study utilizes IHC optogenetic stimulation and SGN recordings, showing that newly formed IHC synapses are indeed functional, exhibiting glutamatergic excitatory postsynaptic currents. When older organs of Corti were plated, synaptic activity probed by deconvolution, showed more mature release properties, closer to the highly specialized mode of IHC synaptic transmission that is crucial for coding the sound signal. This newly developed functional assessment of regenerated IHC synapses provides a powerful tool for testing approaches to improve synapse regeneration.

INTRODUCTION

Inner ear ribbon synapses between inner hair cells (IHCs) and type I auditory nerve fibers (here referred to as spiral ganglion neurons (SGNs)) can be damaged during noise exposure or in the process of aging, this resulting in 'synaptopathy' that can contribute to hearing loss[1,2]. Noise exposure triggers massive glutamate release from IHCs, causing excitotoxicity via postsynaptic glutamate receptors on SGN endings. Several studies have investigated whether ribbon synapses do regenerate post noise-trauma and found that synapse regeneration does occur in several mammalian species[3-6]. In response to damaging noise exposure, SGNs retract from IHCs and can grow back toward IHCs to reform synapses. This regenerative process seems to be highly dependent on the level of sound exposure and can sometimes lead to poor regeneration after noise trauma.

Several studies have used *in vitro* cell-culture models of the cochlea to create new synaptic contacts and study mechanism that might facilitate synapse regeneration[7,8,9]. In one such model, early postnatal cochlear tissue was mechanically denervated and SGNs[10,11] or stem cell-derived neurons[12,13] were placed in co-culture. In such conditions, newly formed contacts between IHCs and newly added SGNs were confirmed by immunolabeling, showing the expression of both pre- and postsynaptic markers. Other studies demonstrated that neuronal progenitors obtained from embryonic stem cells promote ribbon synapse formation, both *in vitro*

65 and *in vivo*[14,15]. Engraftment of embryonic stem-cell-derived otic progenitors into the cochlear
66 nerve trunk of an adult gerbil model of deafness showed fiber growth to the IHCs[14] and a partial
67 restoration of the auditory hearing threshold[16], as measured by auditory brainstem responses
68 (ABRs). Several *in vivo* studies have further demonstrated protection of auditory synapses in a
69 mouse model of noise-induced synaptopathy by genetic[17] or viral[18] delivery of NT3, the
70 neurotrophin receptor agonist amitriptyline[19] or by bisphosphonate[20] before or within a short
71 time-window after noise exposure. An antibody to Repulsive Guidance Molecule A (RGMa) was
72 effective in restoring the synapse when administered onto the round window membrane one
73 week after noise exposure[21]. So far, these studies have only relied on immunolabeling of pre-and
74 postsynaptic markers for identifying newly formed IHC/SGN synapses as well as on ABR
75 measurements. However, a direct functional measurement of the properties of such newly
76 formed synaptic contacts has not been performed. To properly encode the sound signal, ribbon
77 synapses must display fast, reliable and indefatigable synaptic transmission[22]. This is achieved
78 by a complex release machinery[23] associated with non-conventional postsynaptic properties that
79 produce fast and unusually large EPSCs with various waveforms (mono- and multiphasic)[24-26].
80 The goal of this study was to assess the physiological properties of each individual
81 regenerated synaptic contact formed in co-cultures of postnatal mouse denervated organs of Corti
82 and added SGNs. Hair cells were stimulated optogenetically and added SGNs were visualized by
83 expression of fluorescent reporters, so their somata could be targeted for patch clamp recordings.
84 Indeed, newly formed synapses were found to be functional, as light stimulation of hair cells
85 activated glutamatergic synaptic currents in SGNs. Denervated organs of Corti were plated at
86 different ages for co-culture to test if their age affects properties of synaptic transmission.
87 Deconvolution of EPSC waveforms provided a powerful tool to probe for the mode of
88 transmitter release and showed that, when older organs of Corti were plated, synaptic
89 transmission in regenerated synapses showed more mature properties, closer to the specialized
90 mode of native IHC synaptic transmission.
91
92 **MATERIALS AND METHODS**
93 *Animals*

94 All experiments were performed in accordance with protocols approved by the Johns Hopkins
95 University Animal Care and Use Committee. Animals of either sex were used in the experiments
96 indiscriminately. All mouse lines used is this study were maintained on a C57BL/6J background.
97 Cochlear tissue with optogenetically competent auditory hair cells was obtained by crossing
98 Growth Factor independent 1 Cre mice (*Gfi1*$^{Cre/+}$; a gift from Dr. Lin Gan and Dr. Jian Zuo, New
99 York[27]) with homozygous floxed Ai32 mice (*Ai32*$^{fl/fl}$; Channelrhodopsin-2; ChR2; Jackson
100 laboratory, #012569). Cochlear tissue with fluorescent SGNs was obtained from different mouse
101 lines: 1) Microtubule-Associated Protein Tau driving the Green Fluorescent Protein expression
102 (*Mapt-GFP*$^{+/+}$, Jackson laboratory, #029219). MAPT is a protein involved in microtubule
103 assembly and stability in neurons[28]; 2) the Basic Helix-Loop-Helix Family Member BHLHB5
104 Cre mice (*Bhlhb5*$^{Cre/+}$[29,30]) crossed with homozygous floxed Ai9 mice (*Ai9*$^{fl/fl}$; Td-Tomato,
105 Jackson Laboratory #007905) and 3) Bhlhb5Cre/+ mice crossed with homozygous floxed
106 GCaMP6f mice (*GCaMP6f*$^{fl/fl}$; Jackson laboratory, #028865). BHLHB5 is a transcription factor
107 expressed in the central nervous system and in sensory nerve fibers[31].GCaMP6f is a genetically
108 encoded Ca^{2+} indicator where GFP is coupled to the Ca^{2+} binding protein calmodulin. GCaMP6f
109 displayed a basal GFP fluorescence that could be observed by epifluorescence with a 470 nm
110 LED. Therefore, in this study, GCaMP6f was used as a GFP-like fluorescent reporter and not as
111 a Ca^{2+} indicator due to cross interaction with the ChR2 excitation wavelength also at 470 nm.
112
113 *Preparation of denervated organs of Corti for culture*
114 To prepare cultured cochlear tissue including inner and outer hair cells, without remaining
115 connections to spiral ganglion neurons, a technique of culturing cochlear 'micro-isolates' first
116 reported by Flores-Otero et al (2007)[32] and later by Tong et al (2013)[10] was adapted; here called
117 'denervated organs of Corti'. At P3-P5, P7-P8 or P10-11, mice were euthanized, and cochlear
118 tissue was extracted from each temporal bone of *Gfi1*$^{Cre/+}$*; Ai32*$^{fl/+}$ or *Gfi1*$^{+/+}$*; Ai32*$^{fl/+}$ mice, then
119 transferred to a petri dish containing cold Hank's Balanced Salt Solution (HBSS, Thermofisher,
120 #14025-092). The organ of Corti, containing all IHC and OHC rows along with their surrounding
121 supporting cell tissue, was physically 'micro-isolated 'from the connecting afferent SGN fibers
122 and spiral ganglion which includes the SGN somata, with a blade, close to the base of the IHCs.
123 Denervated organs of Corti were obtained from the mid turn of the organ or Corti so that results
124 could be compared between the different sessions. Denervated organs of Corti were then

125 transferred onto coverslips that had been coated with 50 µg/ml of Laminin (Corning, #354232)
126 and poly-L-Ornithine (0.01%, Sigma Aldrich, #P4957) in a 4-well petri dish (Greiner Bio One,
127 #627170) and were cultured in DMEM/F12 – Glutamax (GIBCO, #10565-018) supplemented
128 with N2 (GIBCO, #17502-048), B27 (GIBCO, #17504-044) and 10% Fetal Bovine Serum (FBS,
129 GIBCO, #A3160401) and maintained in a humidified incubator with 5% CO2 at 37°C for 4
130 hours. In a single session, typically 6 littermate mice were sacrificed, and 12 micro-isolates were
131 plated onto 12 coverslips. For this study, 7 such sessions were performed with P_{3-5} cochlear
132 tissue, 2 sessions with P_{7-8} cochlear tissue and 2 sessions with P_{10-11} cochlear tissue.
133
134 *Isolation of primary auditory neurons*
135 SGNs were isolated by using a modified version of the previously described[12]. For fluorescently
136 marked SGNs, either *Mapt-GFP*$^{+/+}$, *Bhlhb5*$^{Cre/+}$*; Ai9*$^{fl/+}$ or *Bhlhb5*$^{Cre/+}$*; GCaMP6f*$^{fl/+}$ mice were
137 used (see Animals section). The cochlea was extracted from the temporal bone and transferred to
138 a petri dish containing HBSS. Spiral ganglion tissue was isolated from six to eight P0-P2 mouse
139 cochleas and pooled in a single tube. Briefly, the organ of Corti was removed from the basal to
140 the apical turn, leaving the SGNs embedded in the soft modiolar connective tissue of the spiral
141 ganglion, that was removed as much as possible before digestion. Spiral ganglion tissues were
142 digested with 500 µl of Trypsin-EDTA 0.25% (GIBCO; #25200-056) and 500 µl of Collagenase-
143 I 0.2% (GIBCO, #17018-029) during 20 min at 37°C. The digestion was stopped by adding 100
144 µl of FBS. The supernatant was carefully removed and replaced with fresh DMEM/F12 –
145 Glutamax medium supplemented with N2, B27, 50ng/ml of Neurotrophin-3 (NT3, Novus
146 biologicals; #NBP1 99227), 50ng/ml of Brain Derived Neurotrophic Factor (BDNF, Novus
147 biologicals; #NBP1 99674) and 10% FBS. The mitotic inhibitor Cytarabine (AraC, 5µM; Sigma
148 Aldrich, #1162002) was added to block glial cell proliferation and improve the SGN culture[33].
149 The antibody anti-Repulsive Guidance Molecule-A (RGMa, 10µg/ml; Thermofisher, #MA5-
150 23977) was added, as it has been shown to promote synapse formation by blocking a repulsive
151 guidance pathway[11]. Spiral ganglion tissues were then mechanically triturated by pipetting up
152 and down several times. Using a cell counting chamber, this protocol allowed to isolate about
153 400.000 SGNs/ml from 8 cochleas. Then, about 30.000 SGNs were added to each well
154 containing one coverslip with one micro-isolated hair cell tissue. The co-cultures were left for 10

155 to 12 days in the incubator until tested for newly formed synapses. During this time, culture
156 medium was exchanged every 1 to 2 days.
157
158 *Electrophysiological recordings*
159 At 10 to 12 days *in vitro* (DIV10 to DIV12), coverslips with co-cultures were placed in a
160 recording chamber filled with an extracellular solution compatible with NMDA receptor
161 activation (in mM): 144 NaCl, 2.5 KCl, 1.3 $CaCl_2$, 0.7 NaH_2PO_4, 5.6 D-Glucose, 10 HEPES and
162 0.03 D-serine pH 7.4 (NaOH), 300 mOsm. Co-cultures were observed with a 40x water
163 immersion objective (CFI60 Apo 40X W NIR, NA = 0.8, W.D = 3.5mm) attached to an upright
164 Nikon A1R-MP microscope.
165 All patch clamp experiments were performed at room temperature using a double EPC10
166 HEKA amplifier controlled by the software Patchmaster (HEKA Elektronik). Patch pipettes,
167 both for hair cell and SGN soma recordings, were pulled using a Flaming/Brown micropipette P-
168 1000 puller (Sutter Instrument) and fire polished with a Micro forge MF-900 (Narishige) to
169 achieve a resistance between 4-7 MΩ.
170
171 *Whole cell patch clamp recording from ChR2$^+$ IHCs*
172 Patch pipettes were filled with an intracellular solution (in mM): 145 KCl, 0.1 $CaCl_2$, 1 $MgCl_2$, 5
173 HEPES, 1 K-EGTA, 2.5 Na_2-ATP, pH 7.4 (KOH), 300 mOsm. The holding membrane potential
174 of IHCs was set at -74 mV (corrected for a liquid junction potential of 4 mV). IHCs of *Gfi1*$^{Cre/+}$;
175 *Ai32*$^{fl/+}$ mice were depolarized by activating channelrhodopsin-2 with a 470 nm blue LED
176 (470/24 nm; 196mW) delivered by a Spectra X light engine (Lumencor Inc, Beaverton, OR)
177 connected to the epifluorescent port of the Nikon A1R-MP microscope. The 470 nm light
178 irradiance delivered through the 40x objective was estimated at 9mW/mm^2 using a DET10A
179 optical power meter (Thorlabs Newton, NJ).
180
181 *Recordings from SGN somata*
182 Patch pipettes were filled with an intracellular solution containing the following (in mM): 110 K-
183 $MeSO_3$, 20 KCl, 0.1 $CaCl_2$, 5 K-EGTA, 5 HEPES, 5 Na_2-phosphocreatine, 5 Mg_2-ATP, 0.3 Na_2-
184 GTP, pH 7.4 (KOH), 300 mOsm. Tetrodotoxin citrate (1-5 µM, #1069), (*RS*)-3-(2-
185 Carboxypiperazin-4-yl)-propyl-1-phosphonic acid ((Rs)-CPP; 20 µM; #0173), an NMDA

186 receptor blocker; 2,3-Dioxo-6-nitro-1,2,3,4-tetrahydrobenzo[*f*]quinoxaline-7-sulfonamide
187 (NBQX; 20 μM; #1044), a glutamate -AMPA/Kainate receptor blocker and CP465-022 (1 μM;
188 #2932), a selective AMPA receptor blocker, were purchased from R&D Systems. While TTX
189 was added in the general perfusion, GluR blockers were locally perfused.
190 The SGN somata to record from, were selected by visualizing the hair cell rows and
191 finding SGN fibers with fluorescing terminals close to the hair cell rows. From such fluorescing
192 SGN endings, fibers were traced back to their somata, where patch recordings were made. SGN
193 somata were randomly found from tens to hundreds of microns away from the hair cell-
194 containing denervated organ of Corti tissue. For voltage clamp intracellular recordings, the
195 holding potential of SGNs was set at -79 mV (corrected for a liquid junction potential of 9 mV).
196 Recordings were included in the analysis if the holding current was < -200 pA at a holding
197 potential of –79 mV, and if the series resistance (Rs) was < 20 MΩ. Recordings were not
198 corrected for Rs.
199 Excitatory postsynaptic currents (EPSCs) were elicited by stimulating hair cells, either by
200 optogenetic hair cell stimulation or by a local application of extracellular solution containing 40
201 mM K^+, (sodium was reduced as potassium was increased). 40 mM K^+-induced stimulation was
202 used when hair cells were ChR2 negative. For some recordings, the absence of synaptic events in
203 response to the optogenetic stimulation was confirmed by application of 40 mM K^+.
204
205 *EPSC analysis*
206 EPSC analysis was mostly performed as described previously[34]. After the baseline holding
207 current was zeroed out, EPSCs were detected using a threshold at a manually-determined level
208 (typically -10 to -20 pA), set by visual examination of data. Compared to EPSCs analyzed in the
209 previous study, recordings obtained here produced EPSCs with smaller amplitudes on average,
210 so it was not possible to find a threshold such that all or most EPSCs would exceed the threshold,
211 while little or no noise did so. The threshold was set to eliminate noise as much as possible.
212 Thus, a significant (and unknown) number of small EPSCs are not included in the data
213 analyzed. A MATLAB routine provided EPSC amplitude, area, 10-90% rise times and 90-10%
214 decay times for 'fast 'EPSCs, both from recordings with purely fast and mixed (fast and slow)
215 EPSCs. Only EPSCs from fast-type recordings were analyzed using deconvolution[34] in which an
216 EPSC is expressed as the sum of one or more kernels. The kernel is the average of' monophasic '

217 EPSCs (defined as having one peak and a mono-exponential decay) from the individual
218 recording, normalized to magnitude 1. An optimum summation of kernels to fit each EPSC is
219 found by varying the amplitude and time delay of each kernel making up the sum. The
220 optimization is done using the lasso method[35], which uses the smallest number of kernels in the
221 sum that produces a good fit to the EPSC waveform (least squares). The fitting process was done
222 with the lasso routine in MATLAB. The assumption is that each kernel represents the release of
223 a bolus of neurotransmitter. This analysis provides an estimate of the number of neurotransmitter
224 releases in an EPSC and their arrangement in time and amplitude. Examples of fits determined
225 with this method are shown in **Fig. 5A2-A5**. The green pulse trains in **Fig. 5A2-A5** show the
226 amplitudes and times of occurrence of the kernels for four example EPSCs. The numbers show
227 the number of kernels needed in each case. If multiple kernels are needed for fitting the EPSC, it
228 is called multiphasic.
229
230 *Immunolabeling*
231 P4-5 *Gfi1*$^{+/+}$*; Ai32*$^{fl/+}$ isolated hair cells were co-cultured with wild-type P1 SGNs until DIV12.
232 Co-cultures were fixed with 100% methanol for 10 min at -20ºC. Next, coverslips were washed
233 with 1X Phosphate Bovin Serum (PBS) and incubated with the blocking buffer containing 15%
234 goat serum during 1h30 at room temperature. Tissues were stained to visualize presynaptic
235 ribbons (Mouse IgG_1 anti-CtBP2, 1:200; BD science: #612044; RRID: AB_399431), hair cells
236 (Rabbit anti-Myosin VI, 1:200; Sigma #M5187; RRID: AB_260563), afferent nerve fibers
237 (Chicken anti-NF200, 1:200; Millipore: #AB5539; RRID: AB_11212161), and the postsynaptic
238 AMPA receptors (Mouse IgG_{2B} anti PAN-GluA1-4, 1:500; Millipore-Sigma: #MABN832).
239 Coverslips were incubated with primary antibodies overnight at 4ºC. Next, coverslips were
240 thoroughly washed with 1X PBS before adding secondary antibodies (1:1000) for 2h at room
241 temperature. The cocktail of secondary antibodies contained Goat anti-IgG_1 Dylight 405
242 (Jackson Immuno Research: #115-477-185; RRID: AB_2632529), Goat anti-Rabbit Alexa 488
243 (Invitrogen: #A11008; RRID: AB_143165), Goat anti-Chicken CF405L (Biotium, custom made)
244 and Goat anti-IgG_{2b} Alexa 647 (Invitrogen: #A21242; RRID: AB_2535811).
245
246
247

248 *Statistics*

249 Statistical tests were performed with GraphPad Prism 9.2 (GraphPad Software, Inc). Data
250 distribution was first tested for normality with a Shapiro-Wilk test. Parametric and non-
251 parametric tests were then selected accordingly. When two populations were compared a
252 student-t-test or a Mann-Whitney test was used. To compare more than two populations, a one-
253 way ANOVA with a Tuckey post-hoc test or a Kruskal-Wallis with a Dunn's post-hoc test was
254 used. The limit of significance was set at $p < 0.05$.

255

256 **RESULTS**

257 *Co-cultures of denervated organs of Corti and isolated SGNs*

258 To create regenerated synapses between hair cells and SGNs after synapse loss, co-cultures of
259 denervated organs of Corti and isolated SGNs were established so that they allowed for new
260 synaptic connections to form (modified from[10, 32]; **Fig. 1A**). Organs of Corti were denervated by
261 cutting along the inner spiral bundle, where SGN endings contact the IHCs (**Fig.1A**, dotted red
262 line). Denervated mid-turn organs of Corti were isolated from *Gfi1*$^{Cre/+}$*; Ai32*$^{fl/+}$ and *Gfi1*$^{+/+}$*;*
263 *Ai32*$^{fl/+}$ (Channelrhodopsin-2; ChR2) mice, at postnatal days (P)3-5. In Gfi1^{Cre}-positive organs of
264 Corti, inner and outer hair cells express Channelrhodopsin-2 **(Fig. 1B),** allowing for hair cell
265 transmitter release to be triggered by optogenetic stimulation. Additionally, in Gfi1^{Cre}-negative
266 organs of Corti, transmitter release was induced by local perfusion of extracellular solution with
267 40 mM K^+ [24].

268 To harvest isolated SGNs, several mouse models with fluorescently labeled SGNs were
269 used indiscriminately: *Mapt-GFP* $^{+/+}$; *Bhlhb5*$^{Cre/+}$; *GCaMP6f*$^{fl/+}$ (includes GFP) and *Bhlhb5*$^{Cre/+}$;
270 *Ai9*$^{fl/+}$ (td Tomato). Recording from such fluorescently labeled SGN somata (**Fig. 1E**) while
271 stimulating hair cell release will assure that recorded synaptic activity originates only from
272 newly formed hair cell/SGN synapses. SGNs were dissociated at P0-2 and added 4 h after the
273 denervated organ of Corti had been plated. Co-cultures were kept for 10-12 days *in vitro* (DIV)
274 before SGN recordings during hair cell stimulation were performed.

275

276 *Optogenetic stimulation depolarizes ChR2*$^+$ *IHCs in culture*

277 Denervated P_{3-5} organs of Corti were cultured and tight-seal, whole-cell recordings were
278 performed from ChR2$^+$ IHCs at DIV10-12, to test the approach for stimulating IHCs (**Fig. 1C,**

279 **D**). The IHC membrane potential was -50 mV (-50.2 ± 4.4 mV; n = 23). One-second-long blue
280 light pulses triggered IHC membrane depolarizations with an initial peak followed by an adapted
281 steady state (**Fig. 1C**). The peak response occurred within 4.6 ± 0.7 ms, and $ChR2^+$ IHCs were
282 depolarized to -26.4 ± 3.8 mV (n = 22). After the initial peak, a steady state value of -42.3 ± 2.3
283 mV was reached with a decay time constant of 7.8 ± 2.4 ms. No response was triggered in $ChR2^-$
284 IHCs (n = 12; data not shown), assuring that depolarization of $ChR2^+$ IHCs was due to ChR2
285 activation.
286 For comparison, recordings were also performed in IHCs of acutely isolated organs of
287 Corti whole mount preparations at P4-5 that had preserved 'native 'IHC synapses and included
288 the spiral ganglion (**Fig. 1D**). Here, the IHC membrane potential was about 15 mV more
289 hyperpolarized (-64.6 ± 5.6 mV; n = 11; $p < 0.0001$, unpaired-t test). $ChR2^+$ IHCs were
290 depolarized to a peak level of -47.4 ± 2.8 mV and a steady state level of -52.8 ± 3.2 mV (n = 4).
291 In 6 of 10 IHCs, light-induced depolarization triggered calcium action potentials (Ca^{2+}-APs)
292 (**Fig. 1D**) and 4 of these IHCs also displayed spontaneous Ca^{2+}-APs between light pulses (**Fig.**
293 **1D**, black arrow). Ca^{2+}-APs have been shown to occur in immature IHCs, before the onset of
294 hearing[36] and are thought to trigger bursting activity in immature auditory nerve fibers, an
295 important mechanism for refining circuitry during development of the auditory pathway[37,38].
296 Such Ca^{2+}-APs were not observed in IHC recordings from P3-5 denervated organs of Corti in
297 culture, even when the IHC membrane potential was hyperpolarized by current injection, to
298 remove sodium channel inactivation (n = 17; data not shown).
299 In summary, although some differences regarding IHC membrane potential and evoked
300 activity pattern were found between cultured and acutely isolated organs of Corti, the results here
301 confirm that optogenetic stimulations of $ChR2^+$ IHCs depolarize the IHC membrane potential
302 substantially, to values that are known to induce transmitter release[39,40].
303
304 *SGNs retain diverse electrical response properties in culture*
305 Electrical response properties of P0-2 isolated SGNs, co-cultured with denervated organs of
306 Corti were tested with SGN soma recordings at DIV10-12 (n = 244), and results gained from
307 three different mouse lines were pooled. SGN somata and fibers were visualized by their
308 fluorescence (**Fig. 1E**). Note that most SGNs tested were unlikely to be connected to IHCs, as
309 described below. The resting membrane potential of cultured SGNs was -64 mV (-64.20 ± 4.58

310 mV; n = 148). The current-voltage relations typically showed robust TTX-sensitive Na^+ inward
311 currents (240/244) and delayed rectifier K^+ outward currents (244/244) (data not shown). In
312 response to a series of 100ms long current injection steps, SGN firing displayed different degrees
313 of adaptation during the current pulse, as described before[41,42,43] (**Fig 1F**). Accordingly, response
314 patterns were grouped into Slowly-Adapting (48%; 78/162) (APs change in size but persist
315 throughout pulse), Intermediately-Adapting (20%; 33/162) (multiple APs at beginning of pulse)
316 and Rapidly-Adapting SGNs (32%; 51/162) (one AP at beginning of pulse). Slowly-Adapting
317 SGNs displayed more negative AP thresholds compared to Intermediately- and Rapidly-
318 Adapting SGNs (-46.87 ± 5.11 mV, n = 75 vs -42.96 ± 5.80 mV, n = 33 vs -43.14 ± 4.92 mV, n
319 = 54; respectively, $p < 0.05$, Kruskal-Wallis). These different SGN response patterns could
320 represent different maturation states of the SGNs[41]. They could also reflect different functional
321 subtypes of SGNs which here persist after DIV10-12. Markowitz and Kalluri (2020)[43] have
322 found a correlation between SGN response pattern and location of SGN contact at the IHC's
323 synaptic pole (pillar versus modiolar), and former studies have connected these sites of contact
324 with different physiological[44] as well as molecular SGN properties[45;46;47].
325
326 *New contacts between SGNs and hair cells appear in co-culture and express AMPA receptors*
327 Earlier work has used immunolabeling of pre- and postsynaptic markers, to show that new
328 synaptic contacts between hair cells and SGNs form in culture[10-11]. For the approach here, culture
329 conditions were modified and two different mouse models instead of one were used for co-
330 culture. Therefore, it was reexamined if new IHC/SGN contacts occur in co-culture.
331 Co-cultures of denervated organs of Corti (P3-5) and isolated SGNs (P0-2) were
332 visualized at DIV10-12 (**Fig. 2A-C**). At that time point, a single row of IHCs and three rows of
333 OHCs could often still be identified by shape and location of the fluorescing hair cells (ChR2-
334 eYFP). From the randomly positioned SGN somata (arrowheads), fibers (in red) extended
335 towards the hair cells and were seen to come into close contact with them. Typically, a single
336 fiber made multiple contacts by branching, either with the same or with several hair cells (**Fig.
337 2A, B**). Often, fibers grew along multiple hair cells, appearing to be making 'en passant 'contacts
338 (**Fig. 2C**). This connectivity pattern is reminiscent of the developmental innervation pattern,
339 where branched fiber endings, contacting the same or multiple hair cells are found at the

340 beginning of the first postnatal week (P0-1) and then start to be refined between P4 and P8 to be
341 fully pruned around the onset of hearing (~P12)[48].
342 Sound signal encoding at hair cell ribbon synapses requires the close association between
343 presynaptic ribbons, where glutamate-filled synaptic vesicles are clustered for release, and
344 postsynaptic AMPA-type glutamate receptors (AMPA-Rs)[12;49-50]. Up until now, hair cell
345 synapses in culture have been identified via the juxtaposition of immunolabeling for presynaptic
346 ribbons (CtBP2, a component of the ribbon protein ribeye) and postsynaptic density markers
347 (like PSD95)[7,10, 11]. AMPA-R labeling in young cultured cochlear tissue has been notoriously
348 difficult and was successful here in a small set of experiments. Co-cultures of denervated organs
349 of Corti (P3-5) and isolated SGNs (P0-2) were immunolabeled at DIV10-12. From 6 different
350 cochlear tissues (3 mice), 26 new synaptic contacts between 18 IHCs and SGN fibers were
351 identified by juxtaposition of CtBP2 and AMPA-R labeling (GluA1-4), providing an average of
352 ~1.5 synaptic contacts per innervated IHC. In such an example (**Fig. 2D**), an afferent fiber
353 labeled with anti-Neurofilament 200 (NF200, white) is seen to meander along a row of IHCs
354 (anti-myosin VI labeling, brown), and making a contact (marked by the dashed square) with the
355 shown IHC. The inset magnifies the marked region of interest and shows the close apposition of
356 CtBP2 and AMPA-Rs in a regenerated synapse. Within the set of immunolabeled tissue samples
357 here, no OHC synapses were identified. However, during live tissue imaging, in a few instances
358 fibers were found in close apposition with OHCs (**Fig. 2C**, arrow). Newly formed OHC synapses
359 have been shown before by immunolabeling, but not after the first week in culture[11].
360
361 *Hair cell stimulation activates glutamatergic synaptic currents with various waveforms in*
362 *regenerated synapses*
363 To test if regenerated synaptic contacts are functional, soma recordings were performed from
364 SGNs in co-culture with the denervated organ of Corti (**Fig 3B**). For comparison, SGN soma
365 recordings were performed at P4-5 in acutely isolated whole-mount preparations that included
366 'native 'IHC afferent synapses (**Fig. 3A)**. Hair cell exocytosis was triggered either by one-
367 second-long pulses of blue light stimulation or by a local perfusion of extracellular solution with
368 elevated K^+ (40 mM) in preparations that did not express Channelrhodopsin in hair cells[25]. Both
369 stimulation methods provided comparable results that were pooled.

370 In SGN recordings with native P4-5 synapses, stimulation of hair cell exocytosis
371 triggered a flurry of exclusively 'fast 'synaptic events (n = 7) with 10-90% rise times, median
372 value of 1.21 ms, and 90-10% decay times, median value of 1.81 ms (149 EPSCs from 7 cells;
373 **Fig. 4C-D)**. These EPSCs were blocked with the AMPA/Kainate-R blocker NBQX (20 mM)
374 combined with the NMDA-R blocker (Rs)-CPP (20 mM) (n = 3) (**Fig. 3A1**), consistent with
375 earlier recordings of AMPA/NMDA-R mediated synaptic currents in 5-7 day-old rat SGNs[51].
376 When denervated organs of Corti were co-cultured with P_{0-2} SGNs, after DIV10-12, 10%
377 of the recordings (38 of 374 SGNs) showed a synaptic response to hair cell depolarization **(Fig.**
378 **3C-E)**. Synaptic responses were divided into 'fast', 'slow 'and 'mixed '(slow and fast combined)
379 groups, based on their EPSC waveforms (**Fig. 3C-E**). 51% (18/33) of recordings consisted of a
380 flurry of 'fast 'EPSCs, with 10-90% rise times of 0.42 ms (median value) and 90-10% decay
381 times of 0.66 ms (3346 EPSCs analyzed from 15 SGNs; **Fig. 4B-D**). These regenerated EPSCs
382 were significantly faster than the native EPSCs (10-90% rise times: $p<0.001$; one-way ANOVA
383 with Tukey's post hoc test and 90-10% decay times: $p<0.05$; Kruskal–Wallis with Dunn's post
384 hoc test **Fig. 4D**). 25% (9/33) of recordings had a 'slow 'response, with a single peak and slow
385 decay occurring during the stimulus (**Fig. 3D**). 10-90% rise time median values were 16.56 ms
386 and 90-10% decay time median values were 55.93 ms (71 EPSCs from 6 cells). 17% of
387 recordings (6/33) showed 'mixed 'responses displaying a slow response superimposed by fast
388 EPSCs (**Fig. 3E**). The time courses of slow and fast components in the mixed responses
389 resembled those occurring in the exclusively slow or fast responses, (median values for slow
390 component: 10-90% rise times of 19.99 ms and decay time constants of 67.32 ms (34 EPSCs
391 analyzed); median values for fast component: 10-90% rise times of 0.47 ms and 90-10% decay
392 times of 0.44 ms (407 EPSCs analyzed from 4 cells). Mixed responses were interpreted to be due
393 to multiple synapses with diverse properties feeding into an individual SGN, based on the
394 findings that afferent endings could make multiple contacts with IHCs (**Fig. 2A-C**).
395 Fast EPSCs in both fast and mixed responses were mediated by AMPA-Rs, as shown by
396 complete block with the specific AMPA-R blocker CP465-022 (1 μM) (n = 6 for 'fast'; n = 2 for
397 'mixed') and supported by complete block with the AMPA/Kainate-R blocker NBQX in
398 additional cells (20 μM) (n = 5 for 'fast'; n = 2 for 'mixed'; **Fig. 3C, E**). Slow responses and
399 slow components of mixed responses were partially or completely blocked by combinations of
400 glutamate receptor blockers in 7 of 8 recordings (**Fig. 3D, E**). CP465-022 (1 μM), NBQX (20

401 μM) and (R_s)-CPP (20 μM; NMDA-R blocker), were used in different sequential combinations,
402 and partial block or lack of block indicated, that AMPA, kainate and NMDA receptors might all
403 be participating in mediating the slow component to different extents, depending on the
404 individual recording. For example, the slow component of the mixed response in **Fig. 3E** is
405 partially blocked by the AMPA/kainate-R blocker NBQX, and completely blocked by adding the
406 NMDA-R blocker (R_s)-CPP. In a different example, the slow component was left unaffected by
407 CP465-022 but completely abolished by NBQX, suggesting the involvement of Kainate-Rs in
408 the slow component. The exact contribution of glutamate receptor subtypes to the slow
409 component was not further investigated; further analysis of this study focused on the waveforms
410 of fast AMPA-mediated EPSCs only (**Figs. 4 and 5**).
411
412 *Hair cell age affects the maturation state of regenerated synapses.*
413 IHC synaptic transmission is highly specialized, and single ribbon synapses show a wide range
414 of EPSC amplitudes with some unusually large EPSC amplitudes and complex EPSC waveforms
415 with single or multiple peaks (mono- and multiphasic)[24,25], which are believed to occur based on
416 more or less coordinate release of multiple release events. On the other hand, OHC synapses, like
417 many AMPA receptor mediated CNS synapses, exhibit smaller single-peaked EPSCs[52].
418 Although the IHC's specialized release mechanism is not completely understood, it is believed to
419 play a crucial role in proper encoding of the sound signal[24,25,26, 34, 53]. Ultimately, regenerated
420 IHC synapses should mimic the native IHC synapse's specialized performance. It is therefore
421 desirable to recreate more mature and possibly IHC-type synaptic transmission in culture as a
422 working model for further improvement of regenerative conditions.
423 Here we tested the hypothesis that the maturation stage of the IHC at the time of plating
424 may affect the maturity and features of new synapses formed in culture. For this purpose,
425 denervated organs of Corti plated at P3-5 for culture were compared to others plated at P7-8 or
426 P10-11. Besides the age of the organ of Corti explant, experimental conditions were the same as
427 used before, including the age of the cultured SGNs (P0-2). Interestingly, when culturing more
428 mature denervated organs of Corti, the percentage of recorded SGNs that displayed synaptic
429 currents in response to hair cell stimulation, increased from 10% (38 of 373; P_{3-5}Reg) to 17.6%
430 (9 of 51; P_{7-8}Reg) and 17.5% (10 of 57; P_{10-11}Reg) **(Fig. 4A)**. Secondly, the percentage of

synapses showing solely fast EPSCs, as 100% in P_{4-5} native synapses do, increased from 48 % with P_{3-5}Reg to 89 % with P_{7-8}Reg and 78 % with P_{10-11}Reg (**Fig. 4B**).

To compare EPSC waveforms in different experimental conditions (**Figs. 4** and **5)**, only recordings with fast EPSCs were analyzed for EPSC 90-10% decay times, amplitudes and areas (area representing the charge of the EPSC) (**Figs 4D-F)**. None of these EPSC waveform properties differed for regenerated synapses cultured with organs of Corti of different ages. However, median 90-10% EPSC decay times of regenerated synapses for all three age conditions were about 2.5 times faster compared to native EPSCs recorded from P4-5 SGNs (P_{4-5} Native:1.81 ms (n = 7; 149 EPSCs); $EPSCs^{(P3-5\ Reg)}$: 0.66 ms (n = 15 ; 3346 EPSCs); $EPSCs^{(P7-8\ Reg)}$: 0.60 ms (n = 8; 7243 EPSCs); $EPSCs^{(P10-11\ Reg)}$: 0.58 ms (n = 6; 8535 EPSCs), $p > 0.99$, Kruskal–Wallis with Dunn's post hoc test; **Fig. 4D**). This difference is illustrated with example EPSC waveforms from a native P_{4-5} synapse (P_{4-5} Native) and from a regenerated synapse with a P_{3-5} denervated organ of Corti (P_{3-5} Reg; $EPSCs^{(P3-5\ Reg)}$;**Fig. 4C**). The presence of faster EPSCs in regenerated synapses might indicate some form of maturation in culture, that could occur by a reduction in the NMDA component as found in early postnatal development[51] and/or a change in AMPA receptor subtype expression, as AMPA receptor mediated EPSCs in SGNs speed up during development[25]. Similarly, amplitudes of $EPSC^{(P7-8\ Reg)}$ and $EPSC^{(P10-11\ Reg)}$ were significantly larger compared to native EPSCs recorded from P4-5 SGNs (P_{4-5} Native; respectively, $p < 0.01$ and $p < 0.05$, Kruskal–Wallis with Dunn's post hoc test), whereas $EPSC^{(P3-5\ Reg)}$ were not ($p = 0.88$, Kruskal–Wallis with Dunn's post hoc test, **Fig. 4E**).

In summary, when older organs of Corti were plated, more synapses showed the more mature 'fast 'responses. However, the basic measures of EPSC waveform like amplitude, area, and decay time, were not obviously affected. To further probe for possible differences, a more detailed analysis of EPSC waveforms was performed next.

EPSC waveforms at synapses regenerated with older IHCs reveal properties closer to mature IHC ribbon synapses

Deconvolution analysis of EPSC waveforms was performed[34], probing for possible changes in the mechanism of release that may occur when synapses mature. Only EPSCs of 'fast 'responses were analyzed. The approach is illustrated in **Fig. 5A1**. This method relies on the averaging of monophasic EPSCs (with a smooth rise, a single peak and exponential decay) to compute a

462 'kernel' that is presumed to reflect a single release event (**Fig. 5A2**). 'Multiphasic 'EPSCs with
463 more complex waveforms, are assumed to be the linear sum of multiple asynchronously-released
464 kernels, representing a varying sequence of neurotransmitter release events (**Fig. 5A3-A5**). The
465 sum of kernels required to fit an EPSC is computed (orange dotted line), using the lasso
466 optimization method[35]. This analysis allows estimation of the timing, number and relative sizes
467 of presumed release events making up an EPSC, as illustrated by the dotted peaks of the green
468 lines in **Fig. 5A**. **Fig. 5A** illustrates that individual recordings can include EPSCs with varying
469 numbers of events (kernels) per EPSC, as indicated by the numbers above the EPSCs.
470 It was shown before that EPSCs recorded in native more mature SGN synaptic terminals
471 have very specialized release properties[24-26, 34]. To illustrate such features, summary data from 2–
472 4-week-old synapses from hearing animals are replotted from Young et al. (2021)[34] in **Figs. 5E, I**
473 (blue dotted lines). For this data set, the areas of EPSCs, representing EPSC charge, remained
474 close to unchanged (only slightly decreasing) with increasing numbers of events per individual
475 EPSC at a given synapse (**Fig. 5I**). This result implies that a fixed amount of neurotransmitter is
476 released for each EPSC and that multiphasic EPSCs reflect the desynchronization of that
477 transmitter release into several boluses. Thus, the amplitude of EPSCs must decrease with the
478 increasing number of events per EPSC as shown in **Fig. 5E**, for the EPSC area to remain
479 unchanged.
480 Results from acutely isolated tissue (P4-5) with immature native synapses are also shown
481 for comparison (P_{4-5} Native; black dashed line in **Fig. 5E, I**); here all recordings were pooled (n
482 = 7; 149 EPSCs), due to the small numbers of EPSCs per recording. The small sample size also
483 causes an uptick in the graphs for values > 6 events per EPSC; these values were not included in
484 the interpretation of the data. For immature native synapses, EPSC area increased with higher
485 numbers of events per EPSC, whereas the EPSC amplitudes stayed about constant (very slightly
486 increased). One interpretation of this result is that additional events in EPSCs may come from
487 additional release pools, increasing area when similarly sized events are added. These data
488 suggest a different mode of transmitter release for early postnatal synapses compared to more
489 mature several weeks old synapses.
490 The deconvolution analysis of EPSCs was performed for the three experimental groups
491 resulting in regenerated synapses (same as in **Fig. 4**), with the denervated organ of Corti plated at
492 P3-5, P7-8 or P10-11. The dependence of EPSC amplitude and EPSC area on number of

493 events/EPSC was plotted for individual recordings (in gray) and averages across recordings (in
494 color) (**Figs. 5B-D; 5F-H**). The averages of every condition were replotted in summary panels,
495 for comparison with data from native immature and more mature synapses (**Fig. 5E, I)**. The
496 slopes of the average traces were calculated by a linear fit to the corresponding data over the
497 range of event numbers 1 to 8 only (illustrated by dotted lines in **Figs. 5B-D, F-H**), not using the
498 noisier data for larger event numbers. Statistical tests were performed to compare P3-5, P7-8 or
499 P10-11, and immature and more mature native synapse results were plotted for qualitative
500 comparison in **Fig. 5**, but not included in the statistical analysis of plotted slopes, as data of
501 native immature synapses had to be pooled providing a single value and as experimental
502 conditions had been somewhat different for native mature compared to regenerated synapses.
503 Interestingly, properties of regenerated synapses created with plating more mature organs
504 of Corti showed a clear trend for both EPSC amplitude and area data in the direction of those
505 from hearing animals with more mature ribbon synapses (**Fig. 5J, K**). With increasing number of
506 events/EPSC, EPSCs$^{(P3\text{-}5\ Reg)}$ amplitudes stayed close to constant, like EPSCs$^{(P4\text{-}5\ Native)}$
507 amplitudes, (**Fig. 5B, E**; light pink line and black dashed line). EPSCs$^{(P7\text{-}8\ Reg)}$ and EPSCs$^{(P10\text{-}11}$
508 $^{Reg)}$ amplitudes decreased with increasing number of evens/EPSC (**Fig. 5C-E,** red and purple
509 lines), and slopes were significantly more negative for both conditions compared to EPSCs$^{(P3\text{-}5}$
510 $^{Reg)}$ ($p < 0.05$ and $p < 0.001$ respectively, one-way ANOVA with Tukey's post hoc test, **Fig. 5J**),
511 trending towards the behavior of more mature native synapses (**Fig. 5E**, blue dotted line).
512 Secondly, with increasing number of events/EPSC, EPSC area increased in the regenerated
513 synapses at all three ages (**Fig. 5F-5H**). EPSCs$^{(P3\text{-}5\ Reg)}$ and EPSCs$^{(P7\text{-}8\ Reg)}$ area data qualitatively
514 resembled more closely those of EPSCs$^{(P4\text{-}5\ Native)}$ and had significantly steeper slopes than
515 EPSCs$^{(P10\text{-}11\ Reg)}$ (**Fig. 5I**; **Fig. 5K;** $p < 0.01$, one-way ANOVA with Tukey's post hoc test). The
516 EPSCs$^{(P10\text{-}11\ Reg)}$ area plot with the older organ of Corti plated, with a shallow slope, trended
517 towards the behavior of more mature native synapses, where EPSC areas are close to constant
518 with increasing numbers of events/EPSC.
519 It has been reported previously that the fraction of monophasic EPSCs in individual recordings
520 increases with postnatal age, (second versus third postnatal week)[25]. However, the three
521 experimental groups with regenerated synapses P3-5, P7-8 or P10-11 did not show significant
522 differences in percentage of monophasic EPSCs ($P_{3\text{-}5}$Reg: 34.35%, $P_{7\text{-}8}$Reg: 34.04 and $P_{10\text{-}11}$Reg:
523 35.64%). A weak trend was found in comparison to immature native EPSCs$^{(P4\text{-}5\ Native)}$ (median:

524 10%), as only EPSCs$^{(P10\text{-}11\ Reg)}$, with the older organ of Corti plated, showed a significantly
525 higher percentage of monophasic EPSCs ($p < 0.05$, Kruskal–Wallis with Dunn's post hoc test),
526 again, trending towards the even higher fraction of monophasic EPSCs (median: 60.50 %) in
527 native synapses from hearing animals[34].
528
529 **DISCUSSION**
530 The study here utilizes IHC optogenetic stimulation and recordings from fluorescing SGNs *in*
531 *vitro*, showing that newly formed IHC synapses are indeed functional, exhibiting glutamatergic
532 excitatory postsynaptic currents and show qualitative release properties reminiscent of native
533 mature IHC synapses. This newly developed functional assessment of regenerated IHC synapses
534 therefore provides a powerful tool for testing approaches and compounds to improve synapse
535 regeneration.
536
537 *Limitations of the in vitro approach.*
538 The *in vitro* approach comes with some limitations. 1) Immature pre-hearing hair cells (P3-11)
539 and SGNs (P0-2) were used, for best survival in culture. These choices will not completely
540 reflect how synapse regeneration might occur in the mature cochlea. However, some important
541 properties were still found intact, even under these conditions: At a prehearing age, IHCs in
542 culture developed properties reminiscent of the specialized IHC release mechanism (see below).
543 SGNs plated at an immature stage still displayed the response properties of diverse subgroups of
544 type-I SGNs[22, 41, 43, 44]. 2) Supporting cells of the Greater Epithelial Ridge were mainly removed
545 when denervating cochlear tissue. However, these supporting cells play important roles during
546 cochlear development (for review[54]), by promoting SGN outgrowth and survival[55-57], modulating
547 intrinsic SGN properties[32, 43, 58] and regulating postnatal cochlear spontaneous activity involved
548 in circuitry refinement[37, 59-61]. 3) IHC Ca^{2+} APs have been shown to regulate ribbon synapse
549 maturation[62-64], but are absent in cultured IHCs. Like the absence of other presynaptic inputs[45, 46,
550 65], this could affect synapse maturation. However, despite these limitations, regenerated synapses
551 exhibited functional glutamatergic transmission, with qualitative properties reminiscent of native
552 mature IHC ribbon synapses, validating the approach for gaining insights into mechanisms
553 underlying synapse regeneration and for testing potential regenerative reagents.
554

555 *Glutamatergic transmission in regenerated synapses.*
556 Native IHC synapses are typically identified by immunolabeling of presynaptic ribbons (CtBP2)
557 and juxtaposed postsynaptic AMPA-Rs[49, 50, 66-68]. Native IHC synaptic currents exhibit 'fast'
558 kinetics on the millisecond scale, unusually large amplitudes and have been shown to be
559 mediated by AMPA-Rs[24-26, 49, 69, 70], and additionally by NMDA-Rs during early postnatal
560 development[51, 71, 72]. Similarly, regenerated IHC synapses *in vitro* showed juxtaposed
561 CtBP2/pan-AMPA-R immuno-puncta and a large fraction of EPSCs with 'fast' AMPA-R-type
562 properties. EPSC waveforms with organs of Corti plated at P3-11 and recorded after DIV10-12,
563 were slightly faster compared to native synapses recorded in whole mount preparations at P4-5,
564 possibly due to further maturation during the time in culture that may have resulted in changed
565 contributions and subunits of NMDARs[51] and AMPA-Rs [25, 73-76].
566 Additional to 'fast' EPSCs, regenerated synapses showed 'slow' EPSCs with a tens of
567 milliseconds time scale for rise and decay times, which based on pharmacology included a
568 varying combination of AMPA-, NMDA- and Kainate-R mediated components. Such slow
569 EPSCs appeared at a higher percentage with the youngest organs of Corti (P3-5) plated,
570 suggesting that this phenotype represents a more immature state of regenerated synapses.
571 Gluk1-5 Kainate-R have been found at mature IHC post-synapses by immunolabeling, and
572 mRNA for Kainate-Rs with subunit specific developmental expression profiles have been found
573 in SGNs[45, 47, 68, 77]. A physiological assessment of the role of and time course of Kainate-R
574 responses at developing or mature IHC synapses, is not available at this point. NMDA-R subunit
575 GluN1 and GluN2a are expressed by developing IHC-SGN synapses[70, 72 78]. During cochlear
576 maturation, GluN1 expression decreases and GluN2a is replaced by GluN2b, 2c and 2d (for
577 review[78, 79]). Interestingly, after excitotoxic-trauma, *in-situ* hybridization revealed the re-
578 expression of the GluN1 subunit in SGNs, and its blockade by pharmacology results in a delay in
579 fiber regrowth and function recovery[80]. Recently, Lithium Chloride, known to downregulate
580 GluN2b subunit expression, injected through the round window 1 day after noise exposure, led to
581 the rescue of ribbon synapses in rats[81]. This indicates that regulation of NMDAR subunit
582 expression may not only be involved during synaptogenesis but also may take part in synapse
583 regeneration. In summary, data from the present study suggest that the expression of different
584 glutamate receptor subtypes may occur during synapse regeneration. Further studies are needed

585 to determine, if the appearance of NMDA-Rs and Kainate-Rs besides AMPA-Rs represents a
586 recapitulation of synapse development, or is specific to the process of regeneration.
587 *Culturing older IHCs results in regenerated synapses with more mature, IHC-like release*
588 *properties.* When older IHCs were cultured with SGNs, a more mature synaptic phenotype was
589 found in regenerated synapses. With older IHCs, a higher percentage of SGNs formed functional
590 synapses, and more such synapses had solely fast EPSCs. With older IHCs, regenerated synapses
591 had significantly larger EPSC amplitudes and a higher percentage of monophasic EPSCs
592 compared to younger native IHC synapses. Similar changes of EPSC properties have also been
593 observed for native ribbon synapses during development[25].
594 IHC transmitter release at mature IHC synapses has been shown to operate by more or
595 less coordinate release of a 'unit/bolus' of neurotransmitter, creating mono- and multiphasic
596 EPSCs[25, 26, 34]. This feature is indicated by EPSC area staying constant with larger numbers of
597 events per EPSC. Interestingly, this property of release is not found when creating regenerated
598 synapses with young IHCs in culture (P3-5), suggesting that in P3-P5 IHCs the coordinate
599 release mechanisms has not developed yet. However, it is impressive that with older IHCs,
600 coordinate release can be recreated in regenerated synapses, even *in vitro*.
601 However, although regenerated synapses *in vitro* showed coordinate transmitter release,
602 EPSC amplitudes were on average up to ~10-times smaller compared to mature native IHC
603 synapses, as well as were those of native your synapses at P4. One simple possible explanation
604 for this difference may be due to the fact that EPSCs in native mature IHC synapses were
605 recorded close to the site of release, in IHC afferent endings[24, 25], whereas in the study here,
606 EPSCs were recorded in SGN somata, likely a couple of hundred micrometer away from the
607 synapse, and transmitted by an immature unmyelinated peripheral axon, as afferent ending
608 recordings in this approach with newly formed fragile synapses are not feasible. Optogenetic
609 IHC stimulation in comparison to IHC depolarization by 40 mM K^+ solution evoked EPSCs with
610 similar amplitudes, and therefore is unlikely to have caused small EPSC amplitudes. To be able
611 to make a clear statement regarding differences in EPSC amplitude, the same type of SGN
612 recording would be needed at different IHC ages and in native and culture conditions.
613
614
615

616 *Other synapse regeneration models.*

617 New insights from functional testing of regenerated cochlear ribbon synapses will also inform
618 other disease models where synapse regeneration is needed for restoring function. For example,
619 in certain pathologies of visual function, photoreceptors may degenerate or lose their ribbon
620 synapses[82]. *In vivo* studies have demonstrated that after transplantation, photoreceptor precursor
621 cells (PPCs) can make new synaptic contacts in a host retina, and in some instances improve
622 visual acuity[83, 84]. Recently, the engraftment of a genetically modified retina derived from human
623 embryonic stem cells (hES cells) restored electrical activity of host ganglion cells in nude rats,
624 based on multi-electrode array recordings[85]. An *in vitro* organotypic retina mouse model allows
625 for checking the functional integration of a graft into host tissue, based on the labeling of specific
626 synaptic proteins[86] . In a cochlear *in vitro* model, neural progenitor cells have been shown to
627 acquire new synaptic connections with hair cells using immunolabeling[12], and the approach
628 reported here will now allow for testing the specific properties of such newly formed synapses.
629 Another promising regenerative strategy is to promote the trans-differentiation of inner
630 supporting cells into cochlear hair cells[87]. In the retina, Müller glial cells could potentially re-
631 enter the cell cycle and be transdifferentiated into neurons (For review[88]). Such newly created
632 sensory cells and peripheral neurons will need to be tested for proper synaptic function.
633 Promoting regeneration in the CNS has been challenging, however, some progress has been made
634 towards nerve growth and sometimes some functional recovery[89, 90]. One example is the blocking
635 of the Repulsive Guidance Molecule A (RGMa). Intrathecal injection of the RGMa antibody has
636 been performed in rats following thoracic spinal cord hemi-section and axonal growth along with
637 function recovery were observed[91]. In the present study RGMa protein was blocked to improve
638 IHC/SGN synapse formation, as shown before[11]. Organotypic cell culture models of cerebral or
639 spinal cord tissues have been used for investigating their 3-D architecture[92], mimicking
640 neurodegenerative disease models[93], testing the functionality of a regenerated network, and most
641 importantly, developing new therapeutical tools[94]. In summary, multiple fields are developing
642 approaches to better inform sensory cell, nerve fiber and synapse regeneration approaches. The
643 present work provides first insights into the functional properties of individual regenerated
644 synapses, and therefore has a high potential to provide new insights and cross-disciplinary
645 exchange with the general regenerative field.
646

647 References

648 1. Liberman, M.C. Noise-induced and age-related hearing loss: new perspectives and
649 potential therapies. *F1000Res* **6**, 927 (2017).
650 2. Liberman, M.C. & Kujawa, S.G. Cochlear synaptopathy in acquired sensorineural
651 hearing loss: Manifestations and mechanisms. *Hear Res* **349**, 138-147 (2017).
652 3. Shi, L. *et al.* Noise induced reversible changes of cochlear ribbon synapses contribute to
653 temporary hearing loss in mice. *Acta Otolaryngol* **135**, 1093-1102 (2015).
654 4. Kaur, T. *et al.* Lack of Fractalkine Receptor on Macrophages Impairs Spontaneous
655 Recovery of Ribbon Synapses After Moderate Noise Trauma in C57BL/6 Mice. *Front*
656 *Neurosci* **13**, 620 (2019).
657 5. Luo, Y. *et al.* Repeated Moderate Sound Exposure Causes Accumulated Trauma to
658 Cochlear Ribbon Synapses in Mice. *Neuroscience* **429**, 173-184 (2020).
659 6. Hickman, T.T., Hashimoto, K., Liberman, L.D. & Liberman, M.C. Cochlear Synaptic
660 Degeneration and Regeneration After Noise: Effects of Age and Neuronal Subgroup.
661 *Front Cell Neurosci* **15**, 684706 (2021).
662 7. Wang, Q. & Green, S.H. Functional role of neurotrophin-3 in synapse regeneration by
663 spiral ganglion neurons on inner hair cells after excitotoxic trauma in vitro. *J Neurosci*
664 **31**, 7938-7949 (2011).
665 8. Han, B.R., Lin, S.C., Espinosa, K., Thorne, P.R. & Vlajkovic, S.M. Inhibition of the
666 Adenosine A2A Receptor Mitigates Excitotoxic Injury in Organotypic Tissue Cultures of
667 the Rat Cochlea. *Cells* **8** (2019).
668 9. Koizumi, Y., Ito, T., Mizutari, K. & Kakehata, S. Regenerative Effect of a ROCK
669 Inhibitor, Y-27632, on Excitotoxic Trauma in an Organotypic Culture of the Cochlea.
670 *Front Cell Neurosci* **14**, 572434 (2020).
671 10. Tong, M., Brugeaud, A. & Edge, A.S. Regenerated synapses between postnatal hair cells
672 and auditory neurons. *J Assoc Res Otolaryngol* **14**, 321-329 (2013).
673 11. Brugeaud, A., Tong, M., Luo, L. & Edge, A.S. Inhibition of repulsive guidance molecule,
674 RGMa, increases afferent synapse formation with auditory hair cells. *Dev Neurobiol* **74**,
675 457-466 (2014).
676 12. Martinez-Monedero, R., Corrales, C.E., Cuajungco, M.P., Heller, S. & Edge, A.S.
677 Reinnervation of hair cells by auditory neurons after selective removal of spiral ganglion
678 neurons. *J Neurobiol* **66**, 319-331 (2006).
679 13. Matsumoto, M. *et al.* Potential of embryonic stem cell-derived neurons for synapse
680 formation with auditory hair cells. *J Neurosci Res* **86**, 3075-3085 (2008).
681 14. Corrales, C.E. *et al.* Engraftment and differentiation of embryonic stem cell-derived
682 neural progenitor cells in the cochlear nerve trunk: growth of processes into the organ of
683 Corti. *J Neurobiol* **66**, 1489-1500 (2006).
684 15. Shi, F., Corrales, C.E., Liberman, M.C. & Edge, A.S. BMP4 induction of sensory
685 neurons from human embryonic stem cells and reinnervation of sensory epithelium. *Eur J*
686 *Neurosci* **26**, 3016-3023 (2007).
687 16. Chen, W. *et al.* Restoration of auditory evoked responses by human ES-cell-derived otic
688 progenitors. *Nature* **490**, 278-282 (2012).
689 17. Wan, G., Gomez-Casati, M.E., Gigliello, A.R., Liberman, M.C. & Corfas, G.
690 Neurotrophin-3 regulates ribbon synapse density in the cochlea and induces synapse
691 regeneration after acoustic trauma. *Elife* **3** (2014).

692 18. Hashimoto, K. *et al.* Protection from noise-induced cochlear synaptopathy by virally
693 mediated overexpression of NT3. *Sci Rep* **9**, 15362 (2019).
694 19. Fernandez, K.A. *et al.* Trk agonist drugs rescue noise-induced hidden hearing loss. *JCI*
695 *Insight* **6** (2021).
696 20. Seist, R. *et al.* Regeneration of Cochlear Synapses by Systemic Administration of a
697 Bisphosphonate. *Front Mol Neurosci* **13**, 87 (2020).
698 21. Nevoux, J. *et al.* An antibody to RGMa promotes regeneration of cochlear synapses after
699 noise exposure. *Sci Rep* **11**, 2937 (2021).
700 22. Kiang, N.Y.S. Discharge patterns of single fibers in the cat's auditory nerve. *M.I.T. Press*
701 (1965).
702 23. Chakrabarti, R. & Wichmann, C. Nanomachinery Organizing Release at Neuronal and
703 Ribbon Synapses. *Int J Mol Sci* **20** (2019).
704 24. Glowatzki, E. & Fuchs, P.A. Transmitter release at the hair cell ribbon synapse. *Nat*
705 *Neurosci* **5**, 147-154 (2002).
706 25. Grant, L., Yi, E. & Glowatzki, E. Two modes of release shape the postsynaptic response
707 at the inner hair cell ribbon synapse. *J Neurosci* **30**, 4210-4220 (2010).
708 26. Chapochnikov, N.M. *et al.* Uniquantal release through a dynamic fusion pore is a
709 candidate mechanism of hair cell exocytosis. *Neuron* **83**, 1389-1403 (2014).
710 27. Yang, H. *et al.* Gfi1-Cre knock-in mouse line: A tool for inner ear hair cell-specific gene
711 deletion. *Genesis* **48**, 400-406 (2010).
712 28. Caillet-Boudin, M.L., Buee, L., Sergeant, N. & Lefebvre, B. Regulation of human MAPT
713 gene expression. *Mol Neurodegener* **10**, 28 (2015).
714 29. Appler, J.M. *et al.* Gata3 is a critical regulator of cochlear wiring. *J Neurosci* **33**, 3679-
715 3691 (2013).
716 30. Meng, X. *et al.* Increasing the expression level of ChR2 enhances the optogenetic
717 excitability of cochlear neurons. *J Neurophysiol* **122**, 1962-1974 (2019).
718 31. Brunelli, S., Innocenzi, A. & Cossu, G. Bhlhb5 is expressed in the CNS and sensory
719 organs during mouse embryonic development. *Gene Expr Patterns* **3**, 755-759 (2003).
720 32. Flores-Otero, J., Xue, H.Z. & Davis, R.L. Reciprocal regulation of presynaptic and
721 postsynaptic proteins in bipolar spiral ganglion neurons by neurotrophins. *J Neurosci* **27**,
722 14023-14034 (2007).
723 33. Schwieger, J., Esser, K.H., Lenarz, T. & Scheper, V. Establishment of a long-term spiral
724 ganglion neuron culture with reduced glial cell number: Effects of AraC on cell
725 composition and neurons. *J Neurosci Methods* **268**, 106-116 (2016).
726 34. Young, E.D., Wu, J.S., Niwa, M. & Glowatzki, E. Resolution of subcomponents of
727 synaptic release from postsynaptic currents in rat hair-cell/auditory-nerve fiber synapses.
728 *J Neurophysiol* **125**, 2444-2460 (2021).
729 35. Tibshirani, R. Regression Shrinkage and Selection via the Lasso. *Journal of the Royal*
730 *Statistical Society. Series B (Methodological)* **58**, 267-288 (1996).
731 36. Kros, C.J., Ruppersberg, J.P. & Rusch, A. Expression of a potassium current in inner hair
732 cells during development of hearing in mice. *Nature* **394**, 281-284 (1998).
733 37. Tritsch, N.X., Yi, E., Gale, J.E., Glowatzki, E. & Bergles, D.E. The origin of spontaneous
734 activity in the developing auditory system. *Nature* **450**, 50-55 (2007).
735 38. Kandler, K., Clause, A. & Noh, J. Tonotopic reorganization of developing auditory
736 brainstem circuits. *Nat Neurosci* **12**, 711-717 (2009).

737 39. Goutman, J.D. & Glowatzki, E. Time course and calcium dependence of transmitter
738 release at a single ribbon synapse. *Proc Natl Acad Sci U S A* **104**, 16341-16346 (2007).
739 40. Vincent, P.F., Bouleau, Y., Safieddine, S., Petit, C. & Dulon, D. Exocytotic machineries
740 of vestibular type I and cochlear ribbon synapses display similar intrinsic otoferlin-
741 dependent Ca2+ sensitivity but a different coupling to Ca2+ channels. *J Neurosci* **34**,
742 10853-10869 (2014).
743 41. Crozier, R.A. & Davis, R.L. Unmasking of spiral ganglion neuron firing dynamics by
744 membrane potential and neurotrophin-3. *J Neurosci* **34**, 9688-9702 (2014).
745 42. Davis, R.L. & Crozier, R.A. Dynamic firing properties of type I spiral ganglion neurons.
746 *Cell Tissue Res* **361**, 115-127 (2015).
747 43. Markowitz, A.L. & Kalluri, R. Gradients in the biophysical properties of neonatal
748 auditory neurons align with synaptic contact position and the intensity coding map of
749 inner hair cells. *Elife* **9** (2020).
750 44. Liberman, M.C. Single-neuron labeling in the cat auditory nerve. *Science* **216**, 1239-1241
751 (1982).
752 45. Shrestha, B.R. *et al.* Sensory Neuron Diversity in the Inner Ear Is Shaped by Activity.
753 *Cell* **174**, 1229-1246 e1217 (2018).
754 46. Sun, S. *et al.* Hair Cell Mechanotransduction Regulates Spontaneous Activity and Spiral
755 Ganglion Subtype Specification in the Auditory System. *Cell* **174**, 1247-1263 e1215
756 (2018).
757 47. Petitpre, C. *et al.* Neuronal heterogeneity and stereotyped connectivity in the auditory
758 afferent system. *Nat Commun* **9**, 3691 (2018).
759 48. Coate, T.M., Scott, M.K. & Gurjar, M. Current concepts in cochlear ribbon synapse
760 formation. *Synapse* **73**, e22087 (2019).
761 49. Liberman, L.D., Wang, H. & Liberman, M.C. Opposing gradients of ribbon size and
762 AMPA receptor expression underlie sensitivity differences among cochlear-nerve/hair-
763 cell synapses. *J Neurosci* **31**, 801-808 (2011).
764 50. Rutherford, M.A. Resolving the structure of inner ear ribbon synapses with STED
765 microscopy. *Synapse* **69**, 242-255 (2015).
766 51. Zhang-Hooks, Y., Agarwal, A., Mishina, M. & Bergles, D.E. NMDA Receptors Enhance
767 Spontaneous Activity and Promote Neuronal Survival in the Developing Cochlea.
768 *Neuron* **89**, 337-350 (2016).
769 52. Weisz, C., Glowatzki, E. & Fuchs, P. The postsynaptic function of type II cochlear
770 afferents. *Nature* **461**, 1126-1129 (2009).
771 53. Niwa, M., Young, E.D., Glowatzki, E. & Ricci, A.J. Functional subgroups of cochlear
772 inner hair cell ribbon synapses differently modulate their EPSC properties in response to
773 stimulation. *J Neurophysiol* **125**, 2461-2479 (2021).
774 54. Kohrman, D.C., Borges, B.C., Cassinotti, L.R., Ji, L. & Corfas, G. Axon-glia interactions
775 in the ascending auditory system. *Dev Neurobiol* **81**, 546-567 (2021).
776 55. Ernfors, P., Van De Water, T., Loring, J. & Jaenisch, R. Complementary roles of BDNF
777 and NT-3 in vestibular and auditory development. *Neuron* **14**, 1153-1164 (1995).
778 56. Farinas, I. *et al.* Spatial shaping of cochlear innervation by temporally regulated
779 neurotrophin expression. *J Neurosci* **21**, 6170-6180 (2001).
780 57. Sugawara, M., Murtie, J.C., Stankovic, K.M., Liberman, M.C. & Corfas, G. Dynamic
781 patterns of neurotrophin 3 expression in the postnatal mouse inner ear. *J Comp Neurol*
782 **501**, 30-37 (2007).

783 58. Zhou, Z., Liu, Q. & Davis, R.L. Complex regulation of spiral ganglion neuron firing
784 patterns by neurotrophin-3. *J Neurosci* **25**, 7558-7566 (2005).
785 59. Tritsch, N.X. & Bergles, D.E. Developmental regulation of spontaneous activity in the
786 Mammalian cochlea. *J Neurosci* **30**, 1539-1550 (2010).
787 60. Clause, A. *et al.* The precise temporal pattern of prehearing spontaneous activity is
788 necessary for tonotopic map refinement. *Neuron* **82**, 822-835 (2014).
789 61. Maul, A. *et al.* The Cl(-)-channel TMEM16A is involved in the generation of cochlear
790 Ca(2+) waves and promotes the refinement of auditory brainstem networks in mice. *Elife*
791 **11** (2022).
792 62. Johnson, S.L., Adelman, J.P. & Marcotti, W. Genetic deletion of SK2 channels in mouse
793 inner hair cells prevents the developmental linearization in the Ca2+ dependence of
794 exocytosis. *J Physiol* **583**, 631-646 (2007).
795 63. Johnson, S.L. *et al.* Position-dependent patterning of spontaneous action potentials in
796 immature cochlear inner hair cells. *Nat Neurosci* **14**, 711-717 (2011).
797 64. Johnson, S.L. *et al.* Presynaptic maturation in auditory hair cells requires a critical period
798 of sensory-independent spiking activity. *Proc Natl Acad Sci U S A* **110**, 8720-8725
799 (2013).
800 65. Stalmann, U., Franke, A.J., Al-Moyed, H., Strenzke, N. & Reisinger, E. Otoferlin Is
801 Required for Proper Synapse Maturation and for Maintenance of Inner and Outer Hair
802 Cells in Mouse Models for DFNB9. *Front Cell Neurosci* **15**, 677543 (2021).
803 66. Khimich, D. *et al.* Hair cell synaptic ribbons are essential for synchronous auditory
804 signalling. *Nature* **434**, 889-894 (2005).
805 67. Wong, A.B. *et al.* Developmental refinement of hair cell synapses tightens the coupling
806 of Ca2+ influx to exocytosis. *EMBO J* **33**, 247-264 (2014).
807 68. Fujikawa, T. *et al.* Localization of kainate receptors in inner and outer hair cell synapses.
808 *Hear Res* **314**, 20-32 (2014).
809 69. Matsubara, A., Laake, J.H., Davanger, S., Usami, S. & Ottersen, O.P. Organization of
810 AMPA receptor subunits at a glutamate synapse: a quantitative immunogold analysis of
811 hair cell synapses in the rat organ of Corti. *J Neurosci* **16**, 4457-4467 (1996).
812 70. Knipper, M. *et al.* Transient expression of NMDA receptors during rearrangement of
813 AMPA-receptor-expressing fibers in the developing inner ear. *Cell Tissue Res* **287**, 23-41
814 (1997).
815 71. Peng, B.G., Chen, S. & Lin, X. Aspirin selectively augmented N-methyl-D-aspartate
816 types of glutamate responses in cultured spiral ganglion neurons of mice. *Neurosci Lett*
817 **343**, 21-24 (2003).
818 72. Ruel, J. *et al.* Salicylate enables cochlear arachidonic-acid-sensitive NMDA receptor
819 responses. *J Neurosci* **28**, 7313-7323 (2008).
820 73. Bellingham, M.C., Lim, R. & Walmsley, B. Developmental changes in EPSC quantal
821 size and quantal content at a central glutamatergic synapse in rat. *J Physiol* **511 (Pt 3)**,
822 861-869 (1998).
823 74. Pickard, L., Noel, J., Henley, J.M., Collingridge, G.L. & Molnar, E. Developmental
824 changes in synaptic AMPA and NMDA receptor distribution and AMPA receptor subunit
825 composition in living hippocampal neurons. *J Neurosci* **20**, 7922-7931 (2000).
826 75. Lu, T. & Trussell, L.O. Development and elimination of endbulb synapses in the chick
827 cochlear nucleus. *J Neurosci* **27**, 808-817 (2007).

828 76. Huang, L.C. *et al.* Synaptic profiles during neurite extension, refinement and retraction in
829 the developing cochlea. *Neural Dev* **7**, 38 (2012).
830 77. Peppi, M., Landa, M. & Sewell, W.F. Cochlear kainate receptors. *J Assoc Res*
831 *Otolaryngol* **13**, 199-208 (2012).
832 78. Traynelis, S.F. *et al.* Glutamate receptor ion channels: structure, regulation, and function.
833 *Pharmacol Rev* **62**, 405-496 (2010).
834 79. Sanchez, J.T., Ghelani, S. & Otto-Meyer, S. From development to disease: diverse
835 functions of NMDA-type glutamate receptors in the lower auditory pathway.
836 *Neuroscience* **285**, 248-259 (2015).
837 80. d'Aldin, C.G., Ruel, J., Assie, R., Pujol, R. & Puel, J.L. Implication of NMDA type
838 glutamate receptors in neural regeneration and neoformation of synapses after excitotoxic
839 injury in the guinea pig cochlea. *Int J Dev Neurosci* **15**, 619-629 (1997).
840 81. Choi, J.E. *et al.* Round-window delivery of lithium chloride regenerates cochlear
841 synapses damaged by noise-induced excitotoxic trauma via inhibition of the NMDA
842 receptor in the rat. *PLoS One* **18**, e0284626 (2023).
843 82. Townes-Anderson, E., Halasz, E., Wang, W. & Zarbin, M. Coming of Age for the
844 Photoreceptor Synapse. *Invest Ophthalmol Vis Sci* **62**, 24 (2021).
845 83. Pearson, R.A. *et al.* Restoration of vision after transplantation of photoreceptors. *Nature*
846 **485**, 99-103 (2012).
847 84. Warre-Cornish, K., Barber, A.C., Sowden, J.C., Ali, R.R. & Pearson, R.A. Migration,
848 integration and maturation of photoreceptor precursors following transplantation in the
849 mouse retina. *Stem Cells Dev* **23**, 941-954 (2014).
850 85. Yamasaki, S. *et al.* A Genetic modification that reduces ON-bipolar cells in hESC-
851 derived retinas enhances functional integration after transplantation. *iScience* **25**, 103657
852 (2022).
853 86. Yanai, A., Laver, C.R., Gregory-Evans, C.Y., Liu, R.R. & Gregory-Evans, K. Enhanced
854 functional integration of human photoreceptor precursors into human and rodent retina in
855 an ex vivo retinal explant model system. *Tissue Eng Part A* **21**, 1763-1771 (2015).
856 87. Li, X.J. & Doetzlhofer, A. LIN28B/let-7 control the ability of neonatal murine auditory
857 supporting cells to generate hair cells through mTOR signaling. *Proc Natl Acad Sci U S A*
858 **117**, 22225-22236 (2020).
859 88. Todd, L. & Reh, T.A. Comparative Biology of Vertebrate Retinal Regeneration:
860 Restoration of Vision through Cellular Reprogramming. *Cold Spring Harb Perspect Biol*
861 **14** (2022).
862 89. Nagappan, P.G., Chen, H. & Wang, D.Y. Neuroregeneration and plasticity: a review of
863 the physiological mechanisms for achieving functional recovery postinjury. *Mil Med Res*
864 **7**, 30 (2020).
865 90. Cooke, P., Janowitz, H. & Dougherty, S.E. Neuronal Redevelopment and the
866 Regeneration of Neuromodulatory Axons in the Adult Mammalian Central Nervous
867 System. *Front Cell Neurosci* **16**, 872501 (2022).
868 91. Hata, K. *et al.* RGMa inhibition promotes axonal growth and recovery after spinal cord
869 injury. *J Cell Biol* **173**, 47-58 (2006).
870 92. Stoppini, L., Buchs, P.A. & Muller, D. A simple method for organotypic cultures of
871 nervous tissue. *J Neurosci Methods* **37**, 173-182 (1991).
872 93. Croft, C.L., Futch, H.S., Moore, B.D. & Golde, T.E. Organotypic brain slice cultures to
873 model neurodegenerative proteinopathies. *Mol Neurodegener* **14**, 45 (2019).

94. Boido, M., De Amicis, E., Mareschi, K., Fagioli, F. & Vercelli, A. Organotypic spinal cord cultures: An in vitro 3D model to preliminary screen treatments for spinal muscular atrophy. *Eur J Histochem* **65** (2021).

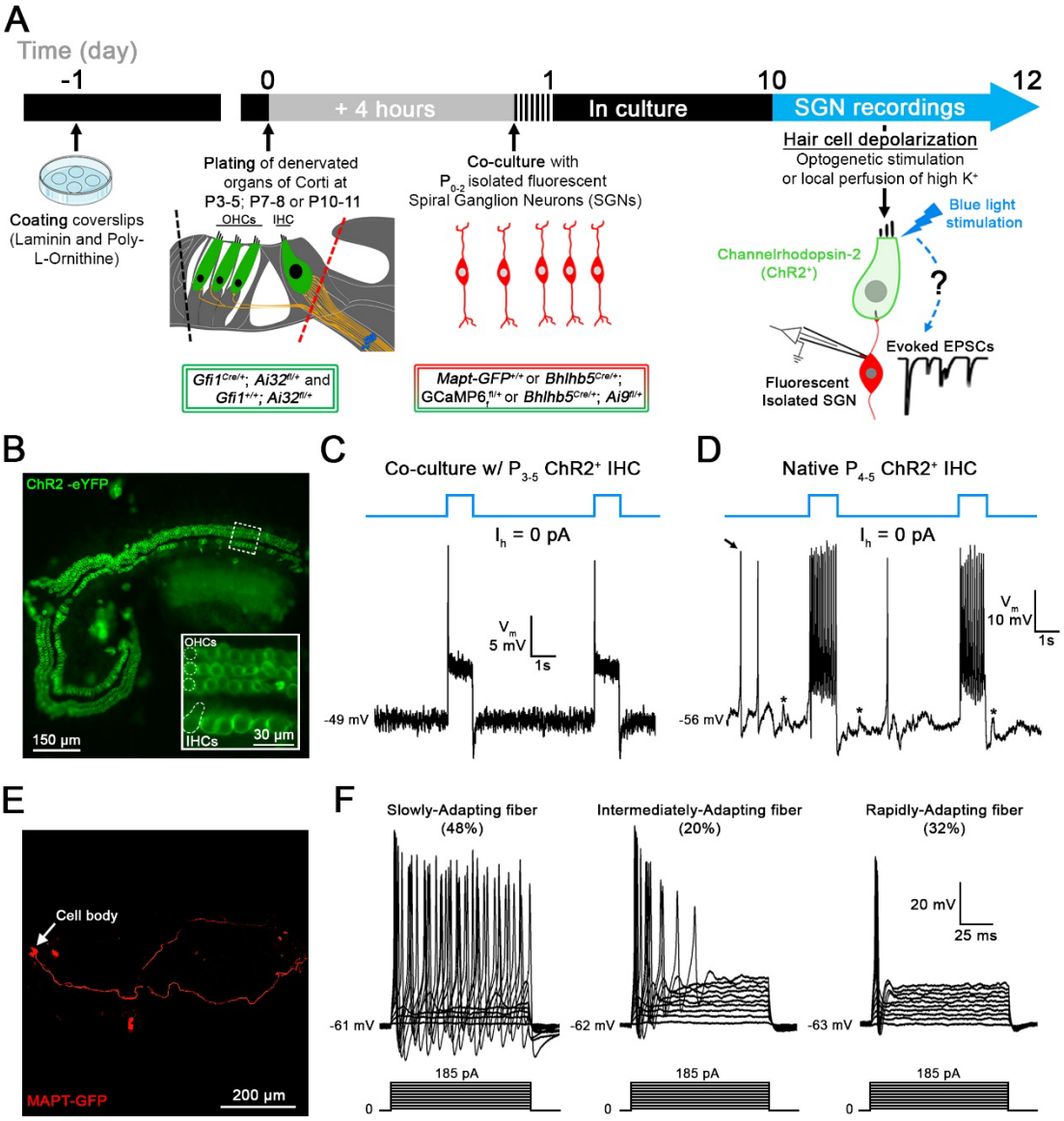

Figure 1. Co-cultures of denervated organs of Corti and isolated spiral ganglion neurons (SGNs) for testing regenerated hair cell synaptic function. A, Organs of Corti were dissected from *Gfi1*$^{Cre/+}$; *Ai32*$^{fl/+}$mice expressing Channelrhodopsin-2 (ChR2) in both inner hair cells (IHCs) and outer hair cells (OHCs) for light stimulation and from *Gfi1*$^{+/+}$; *Ai32*$^{fl/+}$mice, where hair cell stimulation was performed by the local perfusion of 40 mM K^+. Organs of Corti were separated from the lateral wall (black dotted line) and denervated by cutting through SGN endings close to the IHCs, (red dotted line). Denervated organs of Corti were plated at 3 ages, postnatal days (P)3-5, P7-8 or P10-11. Fluorescent SGNs were isolated at P0-2 from one of three mouse lines used indiscriminately (*Mapt-GFP*$^{+/+}$; *Bhlhb5*$^{Cre/+}$; *GCaMP6f*$^{fl/+}$or *Bhlhb5*$^{Cre/+}$; *Ai9*$^{fl/+}$), and co-cultured with denervated organs of Corti. At 10 to 12 days *in vitro* (DIV),

915 recordings were performed from SGN somata while stimulating hair cells. Regenerated
916 functional synapses were identified by excitatory postsynaptic currents (EPSCs) in SGNs in
917 response to IHC stimulation. **B,** Confocal image of a denervated $P_{3\text{-}5}$ *Gfi1*$^{Cre/+}$; *Ai32*$^{fl/+}$ organ of
918 Corti. Inset: ChR2 is observed in IHC and OHC membranes via eYFP tag co-expressed with
919 ChR2. **C,** In current clamp mode, $I_{holding}$ = 0 pA, the IHC membrane potential is recorded in
920 response to two 1s blue light pulses separated by a 4s interval (blue line). Resting membrane
921 potential indicated at the trace. The IHC response includes an initial peak, followed by a steady-
922 state depolarization. **D,** Same protocol as in **C**. IHC recording in a native $P_{4\text{-}5}$ *Gfi1*$^{Cre/+}$; *Ai32*$^{fl/+}$
923 acutely isolated organ of Corti. Light stimulation induces IHC depolarization and superimposed
924 Ca^{2+} APs which are not found in cultured IHCs like in **C**. EPSPs (asterisks) and Ca^{2+} APs (black
925 arrow) also occur spontaneously. **E**, Confocal image of a cultured MAPT-GFP positive SGN
926 with soma and projecting fiber. **F,** SGNs with diverse electrical response properties in culture;
927 'Slowly-Adapting': APs slightly decrease in size throughout the pulse; 'Intermediately-
928 Adapting': multiple APs only at the beginning of the pulse; 'Rapidly-Adapting': single AP at the
929 pulse onset. Current clamp recordings of SGNs; 100ms long current step protocols from resting
930 membrane potential as indicated at trace, with initial 5mV step and subsequent 10mV increasing
931 steps.

932
933
934
935
936
937
938
939
940
941
942
943

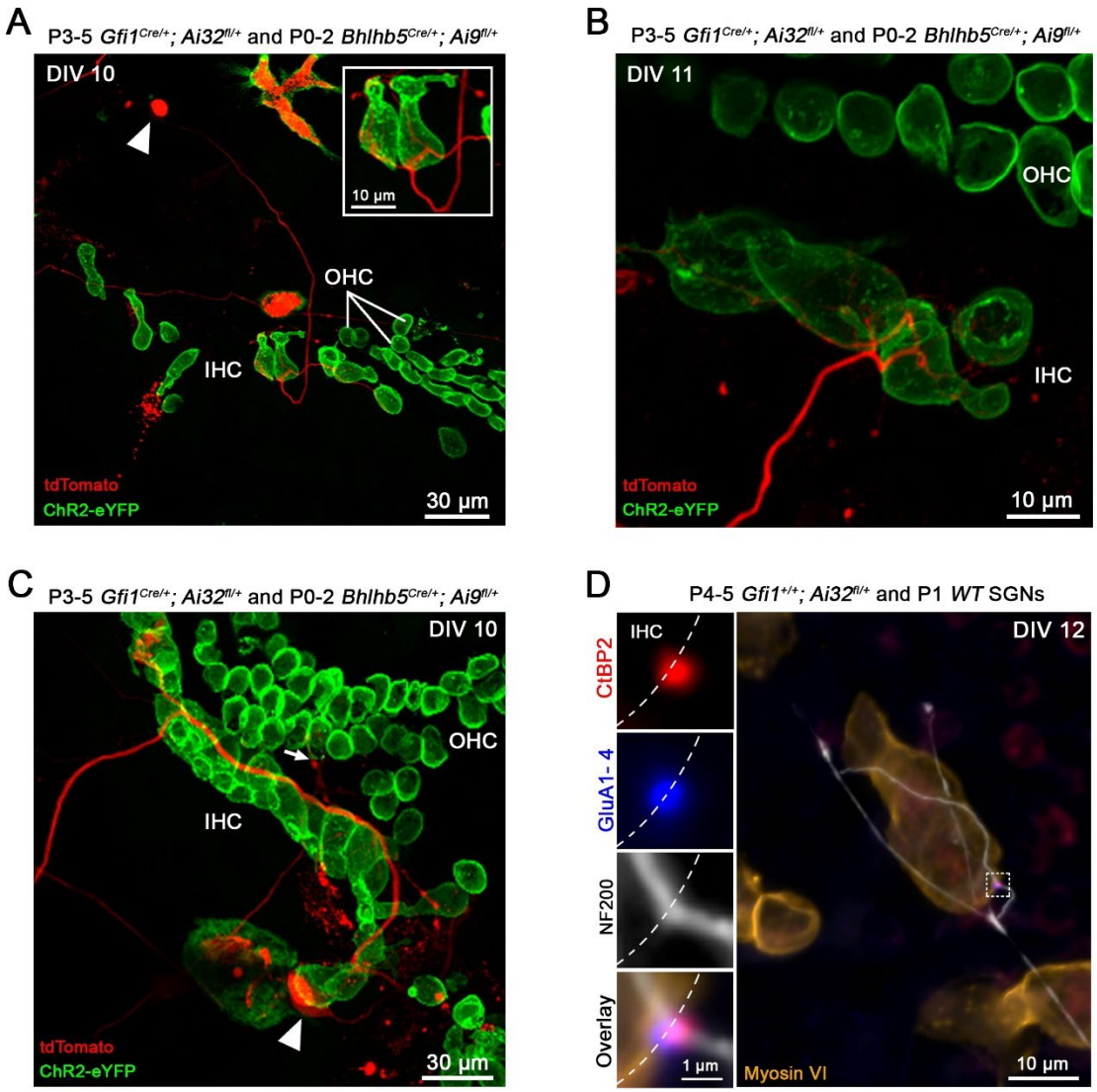

Figure 2. New contacts between hair cells and spiral ganglion neurons appear in co-culture and express AMPA receptors. A-C, Representative examples of live co-cultures at DIV10-11 showing *Bhlhb5*$^{Cre/+}$; *Ai9*$^{fl/+}$, td-Tomato expressing SGN endings (red) close to ChR2^{+} hair cells (green). In **A** and **B**, several IHCs are contacted by multiple endings from a single SGN. Arrowheads in **A** and **C** point to a SGN soma. In **C**, SGN fiber travels along the row of IHCs. Arrow points to a SGN projection reaching the OHC region. **D,** Confocal maximum-intensity projection image from an immuno-labeled co-culture at DIV 12. The insets show individual labels and overlay at a single synapse, with presynaptic ribbon (Anti-CtBP2; red) juxtaposed with postsynaptic AMPA receptors (Anti-PAN GluA1-4; blue). Anti-Myosin VI (orange) labels hair cells and Anti-NF200 (white) labels nerve fibers.

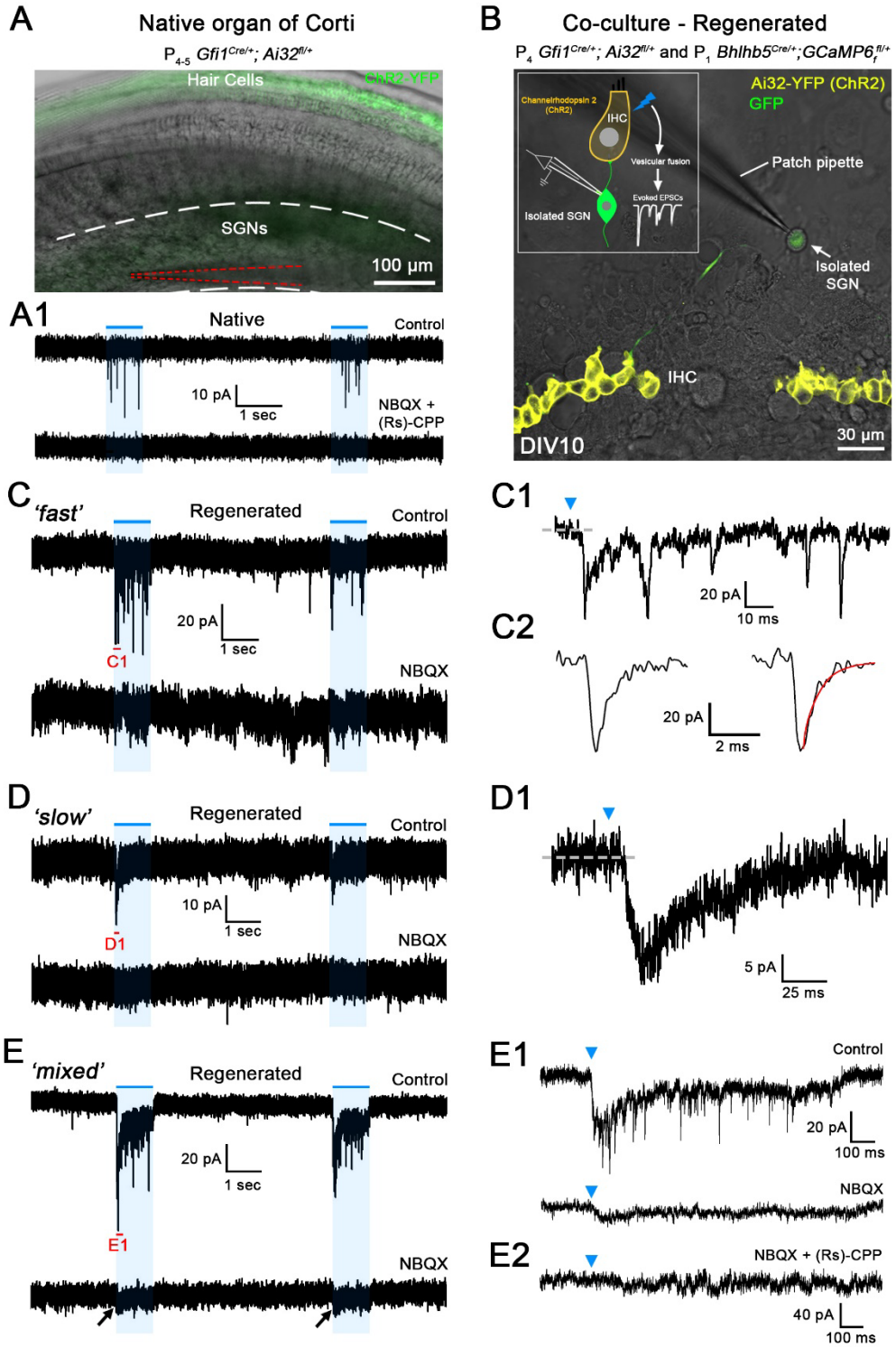

Figure 3. Hair cell stimulation activates glutamatergic synaptic currents with various waveforms in regenerated synapses. A, Superimposed difference interference contrast (DIC) and ChR2-YFP confocal image of a native acutely excised P4-5 *Gfi1*$^{Cre/+}$; *Ai32*$^{fl/+}$ organ of Corti. ChR2^{+} hair cells in green. SG region with SGN somata is located between white dashed lines;

986 recording patch pipette is highlighted by red dashed lines. **A1**, Trace of the SGN recording
987 shown in **A** from a native P_{4-5} synapse, in response to two 1s long light pulses (blue lines).
988 Holding potential -79 mV. A flurry of 'fast 'EPSCs is observed in response to each light pulse
989 (top trace, Control) that are blocked by the combined perfusion of NBQX and (Rs)-CPP (20 µM
990 each), a AMPA/kainate and NMDA receptor blocker, respectively (bottom trace). **B,** A
991 superimposed DIC and ChR2-YFP confocal image of a live co-culture at DIV 10. Row of $ChR2^+$
992 IHCs in yellow. In this example, SGNs express the Ca^{2+} indicator $GCaMP6_f$ (green) under the
993 control of the BHLHB5 Cre promoter. Inset shows a drawing of the experimental setting. **C-E,**
994 Trace examples of SGN recordings of regenerated synapses in co-culture using P_{3-5} denervated
995 organs of Corti, in response to two 1s long light pulses (blue lines). Holding potential -79 mV.
996 **C1-E1** show extended traces of C-E; their extent indicated in red **in C-E**. Blue arrowheads in
997 C1-E1 indicate the beginning of the light pulse. Three response types with different waveforms
998 were found: **C,** 'fast'; **D,** 'slow 'and **E,** 'mixed', the last having both fast and slow responses.
999 Inward currents of all response types were blocked by glutamate receptor blockers; here in the
1000 examples **C1** and **D1** completely by NBQX (20 µM), in **E1** mostly by NBQX, and in **E2**
1001 completely by NBQX and (Rs)-CPP (20 µM).
1002
1003
1004
1005
1006
1007
1008
1009
1010
1011
1012
1013
1014
1015
1016

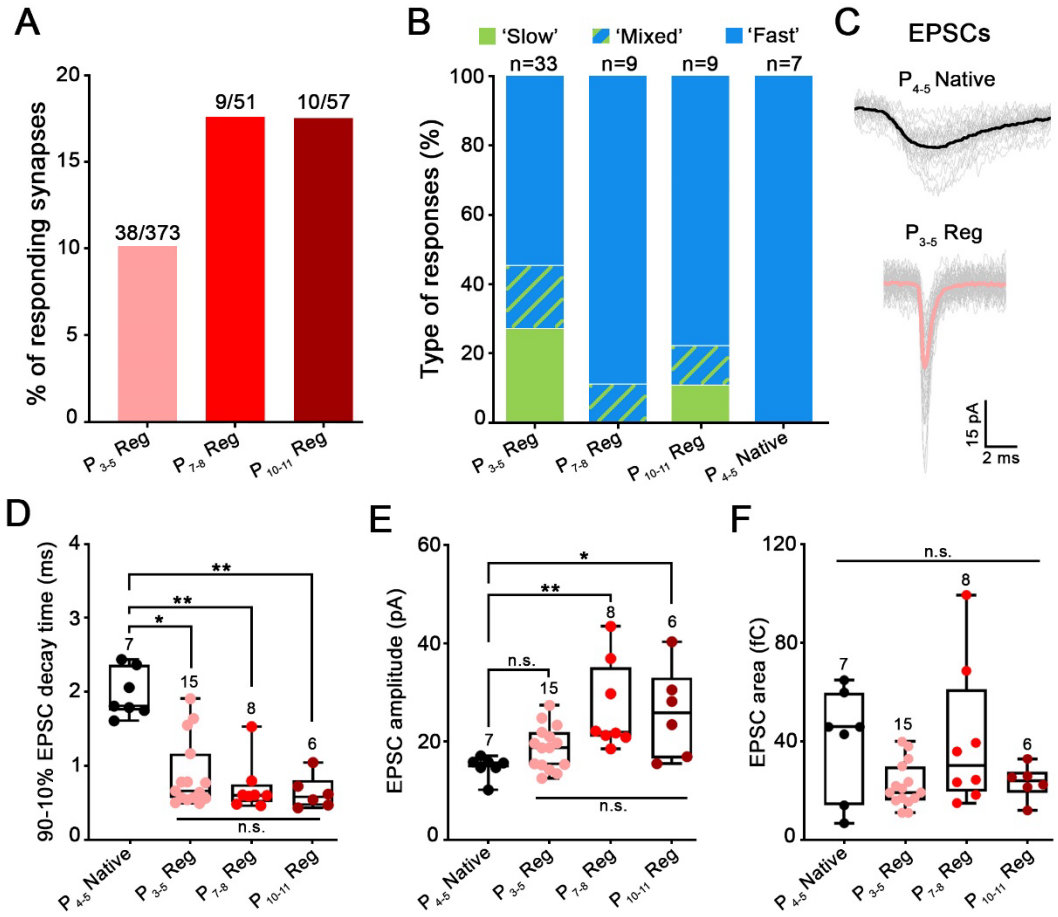

Figure 4. Age of the plated organs of Corti affects the maturation state of regenerated synapses. A-F, Properties of SGN recordings are reported for regenerated synapses in co-cultures of SGNs and denervated organs of Corti, plated at ages P3-5, P7-8 or P10-11; and for native acutely excised P_{4-5} organs of Corti (P_{4-5} Native). **A**, Percentage of SGN recordings showing regenerated postsynaptic activity in response to hair cell stimulation is higher in P_{7-8} or P_{10-11} versus P_{3-5} cultures. **B,** Distribution of 'fast', 'slow 'and 'mixed 'responses (as shown in Fig. 3) of regenerated synapses in comparison to P_{4-5} Native synapses. Contribution of 'fast responses is higher in regenerated synapses of P_{7-8} or P_{10-11} versus P_{3-5} cultures, and 100% in P_{4-5} Native synapses. **C,** EPSC waveform of a P_{4-5} Native synapse (black) is slower that EPSC waveform from a P_{3-5} regenerated synapse (pink; P_{3-5} Reg). Individual waveforms are shown in grey and averaged in black or pink. Holding potential -79 mV. **D-F**, Comparison of EPSC waveform parameters for regenerated and native synapses. Each data point represents the median value from an individual recording. Numbers above each box indicated the number of SGN recordings used for analysis. Boxes represent the median (horizontal line), 10th and 90th

percentile. Whiskers represent maximum and minimum values of the distribution. *$p<0.05$, **$p<0.01$, n.s.: not significant, Kruskal–Wallis with Dunn's post hoc test. **D**, 90-10% median decay time of native EPSCs ($EPSCs^{(P4\text{-}5\ Native)}$; 1.81ms; n=7) were slower compared to regenerated EPSCs of all age conditions: $EPSCs^{(P3\text{-}5\ Reg)}$ (0.66ms; n=15; $p<0.05$); $EPSCs^{(P7\text{-}8\ Reg)}$ (0.60ms; n=8; $p<0.01$) and $EPSCs^{(P10\text{-}11\ Reg)}$ (0.58ms, n=6; $p<0.01$). However, decay time was not statistically different between regenerated EPSCs of all age conditions. **E,** The median amplitude of native EPSCs ($EPSCs^{(P4\text{-}5\ Native)}$: 15.59pA; n=7) was similar compared to $EPSCs^{(P3\text{-}5\ Reg)}$ (18.72pA; n=15). However, $EPSCs^{(P4\text{-}5\ Native)}$ were significantly smaller when compared to $EPSCs^{(P7\text{-}8\ Reg)}$ (21.89pA; n=8; $p<0.01$) and to $EPSCs^{(P10\text{-}11\ Reg)}$ (25.77pA; n=6; $p<0.05$). **F,** The median area of native EPSCs ($EPSCs^{(P4\text{-}5\ Native)}$; 46.00fC; n=7) was similar compared to regenerated EPSCs at all age conditions: $EPSCs^{(P3\text{-}5\ Reg)}$ (19.27fC; n=15), $EPSCs^{(P7\text{-}8\ Reg)}$ (30.25fC; n=8) and $EPSCs^{(P10\text{-}11\ Reg)}$ (24.00fC; n=6). Regenerated EPSCs also displayed similar area values at all age conditions.

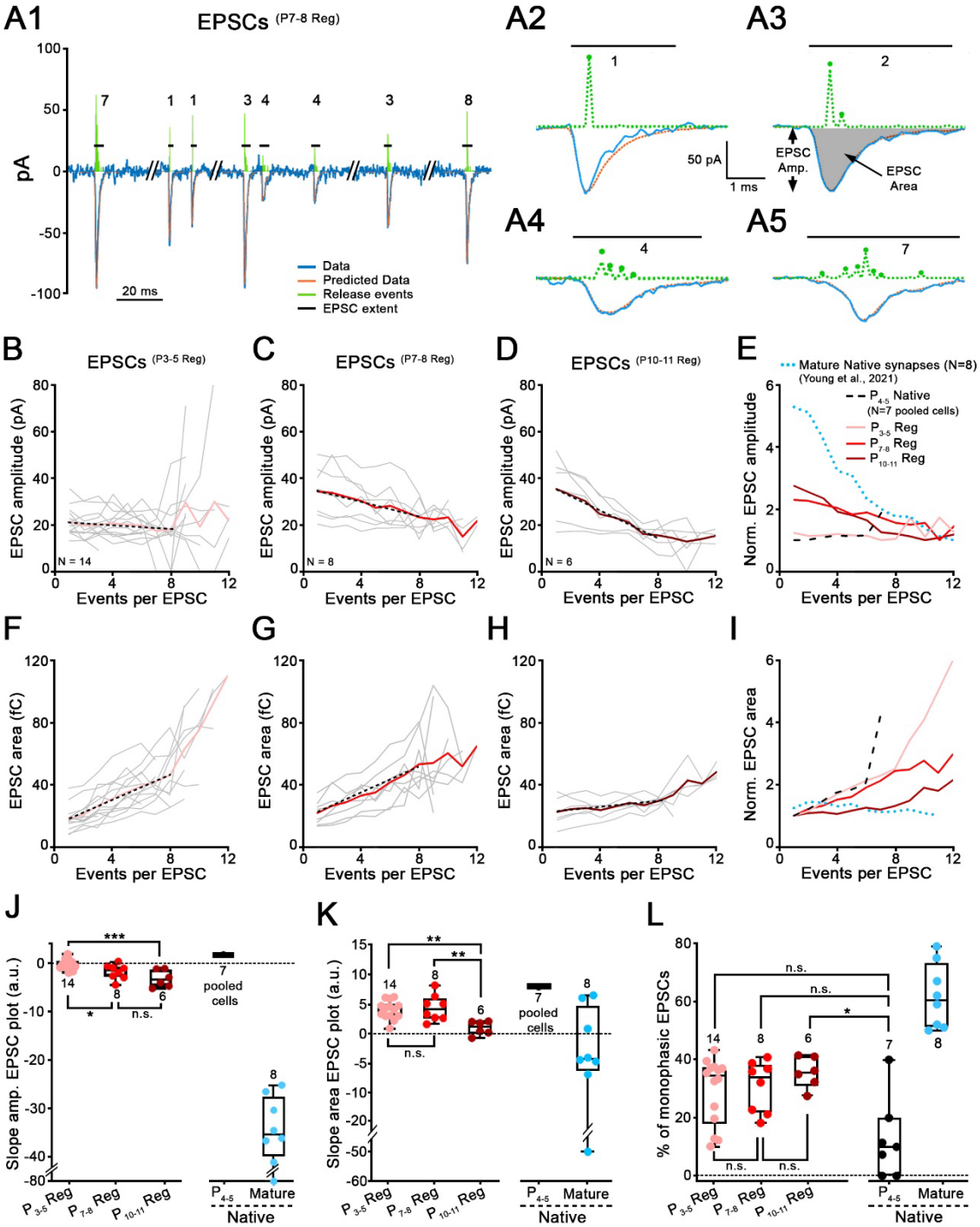

Figure 5. EPSC waveforms at synapses regenerated with older IHCs reveal properties closer to mature IHC ribbon synapses. A, Modeling of EPSC waveforms using deconvolution. **A1,** Trace (blue line) of a SGN recording with 8 exemplar EPSCs$^{(P7\text{-}8\ Reg)}$ recorded from a regenerated synapse. Holding potential: –79 mV. $P_{7\text{-}8}$ denervated organ of Corti was plated for this co-culture with $P_{0\text{-}2}$ SGNs. Four EPSCs from this recording are shown on extended time

scales in **A2-A5** (blue lines). **A2,** Monophasic EPSCs like this example, were averaged to create a kernel (standardized release event) for individual recordings. Kernels (amplitude and time-of-occurrence) are depicted in green dashed line above each EPSC. The fits calculated from the event sequences are shown in orange. EPSC amplitude (EPSC Amp.) and EPSC area (grey filled area) are defined in **A3**. Horizontal black lines represent EPSC extent and numbers indicate the smallest number of events (i.e., kernels) that best fit this EPSC. **B-D,** Mean values of regenerated EPSC amplitude are plotted against the number of events per EPSC, for three co-culture conditions, P_{3-5} (**B,** n=14 synapses, pink), P_{7-8} (**C,** n=8 synapses, red) and P_{10-11} (**D,** n=6 synapses, purple) denervated organ of Corti. Grey thin lines represent individual recordings and bold colored lines represent the averages. Black dotted lines represent the fit of the data, including only data with 1-8 events per EPSC, providing the slope values in **J**. **E**, EPSC amplitude versus events/EPSC plots were normalized to their minimum value and superimposed for different conditions. These include average traces for regenerated synapses from **B-D, (**P_{3-5} Reg, P_{7-8} Reg, P_{10-11} Reg; pink, red and purple), for immature P_{4-5} Native synapses (black dashed lines) and mature ribbon synapses (blue dotted lines, data from[34]). For $EPSCs^{(P4-5\ Native)}$, EPSCs from the 7 recordings were pooled. **F-I,** Same as **B-E**, but with EPSC area plotted against number of events per EPSC. **J,** Slopes of the EPSC amplitude versus the number of events per EPSC calculated from **B-E**, are shown for each condition. $EPSCs^{(P4-5\ Native)}$: 1.79 (n=7 pooled cells); $EPSCs^{(P3-5\ Reg)}$: -0.32 (n=14); $EPSCs^{(P7-8\ Reg)}$: -1.44 (n=8); $EPSCs^{(P10-11\ Reg)}$: -3.26 (n=6) and $EPSCs^{(mature\ native)}$: -35.76 (n=8; data from[34]). One-way ANOVA with Tukey's post hoc test. **K,** Slopes of the EPSC area versus the number of events per EPSC calculated from **F-I**, are shown for each condition. $EPSCs^{(Native\ P4-5)}$: 8.00 (n=7 pooled cells); $EPSCs^{(P3-5\ Reg)}$: 4.33 (n=14); $EPSCs^{(P7-8\ Reg)}$: 4.01 (n=8); $EPSCs^{(P10-11\ Reg)}$: 1.7 (n=6) and $EPSCs^{(mature\ native)}$: -4.32 (n=8; data from[34]). One-way ANOVA with Tukey's post hoc test. **L,** Percentage of monophasic EPSCs per recording is shown for each condition. $EPSCs^{(Native\ P4-5)}$: 10% (n=7); $EPSCs^{(P3-5\ Reg)}$: 34.35% (n=14); $EPSCs^{(P7-8\ Reg)}$: 34.04% (n=8); $EPSCs^{(P10-11\ Reg)}$: 35.64% (n=6) and $EPSCs^{(mature\ native)}$: 60.50% (n=8; data from[34]). Kruskal–Wallis with Dunn's post hoc test. **J-L**, Each data point represents an individual recording. Number of SGN recordings used for analysis is indicated. Boxes represent the median (horizontal line), 10th and 90th percentile. Whiskers represent maximum and minimum values of the distribution. *p<0.05, ***, **p <0.01, p<0.001, "n.s.": not significant.